

Light-Induced Organic Transformations by Covalent Organic Frameworks as Reticular Platforms for Selective Photosynthesis

Paolo Costa,* Alberto Vega-Peñaloza, Leonardo Cognigni, and Marcella Bonchio*

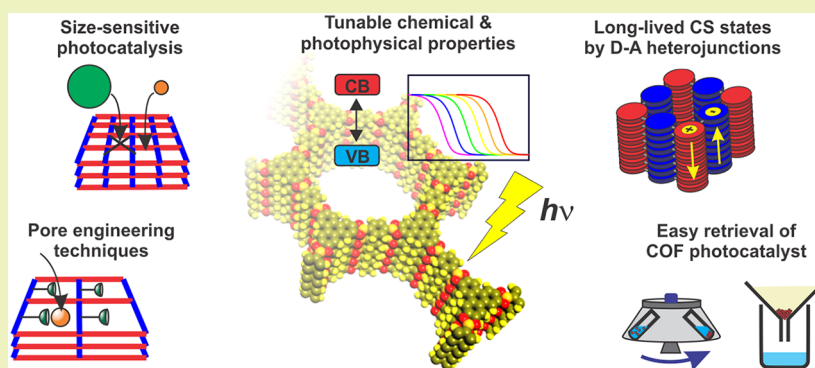
Cite This: *ACS Sustainable Chem. Eng.* 2021, 9, 15694–15721

Read Online

ACCESS |

Metrics & More

Article Recommendations



ABSTRACT: Photoassisted synthesis of value-added organic products has developed greatly in the last decades in response to the pressing need for a transition toward sustainable processes and renewable energy. One of the formidable challenges of the light-induced chemical steps is provided by the control of the catalytic efficiency and selectivity under photocatalytic conditions. An attractive perspective is foreseen by triggering the photoreaction events in confined spaces, wherein light harvesting and photocatalytic units are framed into functional architectures. Division of tasks among specialized compartments responds to a bioinspired strategy with the final aim to orchestrate the rate of concurrent and sequential events, to maximize performance while directing the reaction selectivity. Covalent organic frameworks (COFs) are a class of emerging materials that can meet these requirements, with the potential to bridge the existing gap between molecular and heterogeneous photocatalysis. Here, a rich pool of molecular building blocks and chemical linkages is available to afford crystalline porous solids with tailored photophysical properties emerging from the interconnected COF structure walls, while catalytic cofactors can be provided by engineering of the pore surface. In this Perspective, we highlight recent developments where COFs have been successfully employed as photocatalysts for selective organic transformations. The relationship between the COF reticular structure and its photocatalytic behavior is discussed, in terms of the light-conversion pathways and photoredox events, including electron and/or energy transfer mechanisms. The possible role of confinement effects, intrinsic in long-range order porous COF materials, remains largely unexplored in photocatalytic applications. New progress is expected to arise from close interdisciplinary cooperation involving synthetic chemistry and materials science communities.

KEYWORDS: Covalent organic frameworks, Photocatalysis, Space-confined reactions, Functional porous materials, Organic synthesis, Visible light, Organic semiconductors

INTRODUCTION

The remarkable performance, kinetic control, and selectivity of molecular transformations that occur in natural processes under mild conditions provide a unique paradigm for sustainable processes engineered under an abiotic environment. The outstanding activity of natural systems hinges on specifically evolved catalytic sites in enzymes, which, on one side, facilitate the encounter of the substrates and, on the other hand, constrain the reactants in a tailored activation environment that cooperates to minimize the overall energy requirements. The importance of highly organized functional

architectures is also well-observed in both Photosystem I and II (PSI and PSII), the two pigment–protein supercomplexes responsible to convert and store the solar energy in chemical bonds of energy-rich compounds, e.g. ATP. Natural photo-

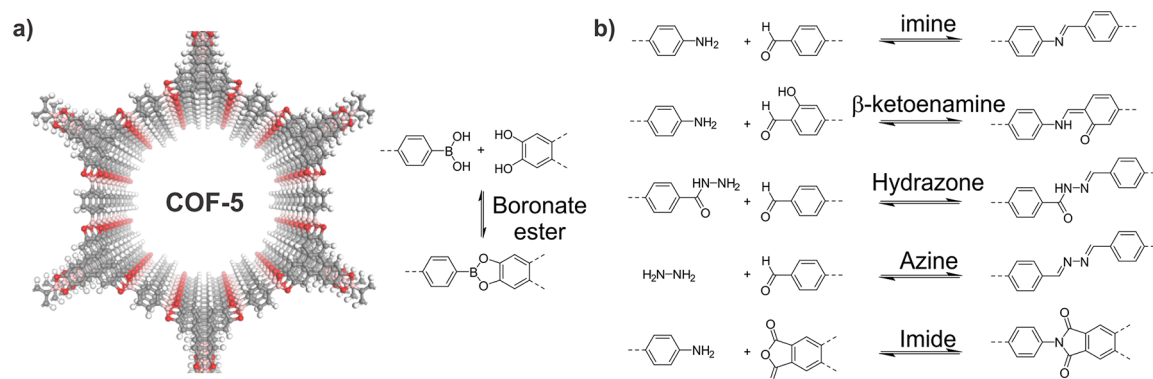
Received: August 12, 2021

Revised: October 21, 2021

Published: November 17, 2021



Chart 1. (a) COF-5 Structure Based on the Reversible Formation of Boronate Ester. (b) Most Popular Dynamic Covalent Chemistry Employed for the Synthesis of COFs



systems share a similar organization where the colocalization of multichromophoric antennas with reaction centers (RCs) allows a highly efficient light harvesting (LH) and energy conversion by orchestrating a cascade of photochemical events.^{1,2}

The grand challenge of artificial photosynthesis (AP) is to replicate the natural photosynthetic functions by creating bioinspired molecular systems and materials capable of exploiting the enormous potential of solar light with the final aim to produce solar fuels and/or value-added organics to feed the world needs for sustainable energy, food, and chemicals.

With this aim, an attractive strategy relies on photoredox catalysis requiring two fundamental components: (i) an LH/RC module consisting of a molecular sensitizer and/or a photoactive semiconductor, and (ii) a redox catalytic manifold targeting a specific reaction.^{3–6} To this aim, the knowledge acquired on the light-induced events occurring in natural photosystems has been recently translated in the field of both homogeneous and heterogeneous photocatalysis applied to selective organic synthesis.^{7,8} Prominent examples deal with the combination of organic dyes or transition metal-based sensitizers with molecular catalysts triggering multiple and sequential photoinduced electron transfer. Along with these photoredox cycles, key intermediates are generated that can induce diverse functional group transformations including selective oxidation, amination, carbon–carbon coupling, and C–H activation.^{9–13} A priority goal in the field is to develop photoinduced asymmetric reactions by controlling the 3D-spatial arrangement of the light-generated reactive intermediates.¹⁴ Milestone results have been achieved via photoactivated chiral catalysts giving rise to enantioselective photoredox cycles.^{15,16} In this direction, an attractive perspective can be envisaged by the molecular engineering of confined spaces featuring the colocalization of phototriggers (LH/RC units) and catalysts within a chiral environment, thus inducing stereoselectivity. Performing the photosynthetic reactions in confined spaces responds to a bioinspired strategy, mimicking the multifunctional catalytic pocket of natural enzymes. In this context, several works in the literature involve organized reaction environments shaped to improve the performance and selectivity of photochemical processes, including, among others, mesoporous inorganic materials, metal–organic frameworks, microemulsions, micelles, foams, and gels.^{17–20}

Here, we highlight the growing field of covalent organic frameworks (COFs) as a promising strategy in reticular chemistry to regulate and control photocatalytic events applied

to small-molecule transformations and selective synthesis. Indeed, notable progress has been reported where COF-based systems are applied to photoassisted H₂O splitting, CO₂ reduction, and hydrogen evolution for solar fuel production.^{21–24} The COF advantage is 2-fold: (i) the periodic organization of chromophore arrays, shaping the COF walls and integrating both LH and RC domains, (ii) a multilevel (2D, 3D) ordered and porous architecture that can enhance the efficiency and selectivity via pore-confined photocatalysis. In addition to the high diversity of building blocks amenable to photoactive COFs engineering, convenient post-functionalization strategies can be applied to the resulting COF backbone and pore walls so to implement recognition, proximity, second-sphere effectors (hydrogen bonding, Lewis bases, orbital steering, etc.), enantioselective catalysis.²⁵

Indeed, COFs are low-density crystalline porous frameworks built from molecular precursors with organic linkers shaped through a reversible covalent bond formation. Since the pioneering work of Yaghi et al. in 2005 (Chart 1a),²⁶ prominent COF structures have been prepared and tested in diverse areas, including energy materials and gas storage,^{22,27} heterogeneous catalysis,^{28,29} stimuli-responsive systems,^{30,31} drug delivery,³² optoelectronic devices,^{33,34} and sensing.³⁵ The great versatility of COF frameworks stems from the possibility to preconfigure their structure, topology, dimensionality, and porosity based on the selected molecular building blocks and their linkers. Therefore, COF synthesis can be rooted within a broad toolbox of organic synthesis methods, so that modular and structural diversity can be generated, affording an unprecedented level of molecular control on the resulting photophysics and the emergent photocatalytic performance. In particular, the geometry of selected organic linkers dictates the possibility of 2D- or 3D-COF formation. In the former case, π -conjugated sheets of 2D-COF are hierarchically assembled by π – π stacking interaction, whereas in 3D-COF, the overall structural backbone is maintained by covalent bonds expanding in a three-dimensional space. For both types of frameworks, the structural stability depends on the chemical linkage, whose choice must guarantee thermodynamic reversibility to yield the most stable, crystalline COF structure. The first-used COF linking groups, based on boroxine and boronated bonds, were plagued from poor chemical stability (e.g., cleaved by hydrolysis), several others linkers have now been successfully incorporated, resulting in more robust frameworks based on imine, β -ketoenamine, hydrazone, azine, and imide-type linkages, among others (Chart 1b).³⁵

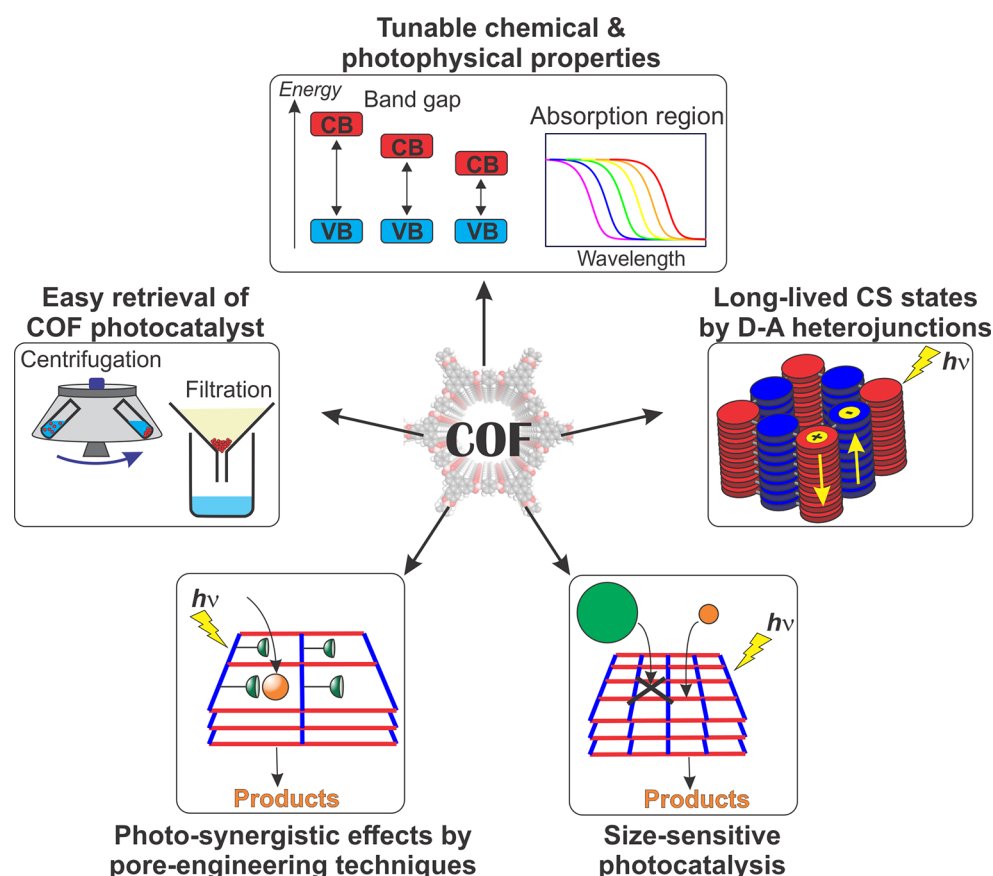


Figure 1. COFs multifunctional properties within photocatalytic applications.

In this context, COFs encompass a series of features that can take the best of both molecular and heterogeneous photocatalysis while bridging the gap between these two worlds by (i) a facile construction of photoresponsive frameworks whose chemical and photophysical properties (e.g., absorption, emission, and band gap) can be easily tailored and optimized, according to the target reaction, (ii) engineering of framework integrated heterojunctions, where electron-donor/acceptor building blocks are assembled into bicontinuous π -columnar arrays enabling long-lived charge separation (CS) states, (iii) the combination of a porous matrix with a photoactive framework ensures a maximized surface area as well as enhanced substrate recognition and selective transport, depending on the pore-dimensions, (e.g., size-selective photocatalysis) and also on the pore-walls hydrophobic/hydrophilic properties, (iv) post-functionalization of the COF backbone and pore walls, which is instrumental for inserting additional functions to meet the LH/RC photodynamics and/or to leverage site-selective and stereoselective processes, (v) straightforward separation/recovery of the COF photocatalyst by simple and inexpensive operations, e.g., centrifugation and filtration (Figure 1).

In this Perspective, we emphasize the development of COFs as a promising platform for photocatalytic applications by summarizing the recent works where COFs have been successfully employed in photodriven organic transformations (Table 1). Herein, the performance of COF-based photocatalysts has been highlighted for selected reaction types (oxidation, reduction, carbon–carbon bond formation) to pinpoint the “ins and outs” of state-of-the-art systems tracing the pathway for the next-generation upgrade. Special attention

is dedicated to the impact of the long-range ordered and porous structure of COFs on the resulting photocatalytic performance.

■ COFs AS PHOTOCALYSTS FOR ORGANIC TRANSFORMATIONS

Covalent organic frameworks (COFs) made of highly π -conjugated building blocks and featuring a π -extended ordered arrangement favor a diffuse π -electron delocalization and transport. For this reason, they are considered as the new frontier of organic semiconductors (OSCs), combining a broad absorption cross-section with photoconduction. By virtue of these properties, COFs have been employed as photocatalysts in light-driven organic transformations as outlined in the seminal case studies reported herein. The photocatalytic properties of COFs are generally discussed in terms of their absorption edge and of the corresponding optical band gap: i.e., by evaluating (i) the wavelength of electron photoexcitation from the valence band (VB) to the conduction band (CB) of the COF materials, and (ii) the energetic positioning of the band edges that define the redox potentials of photogenerated electrons and holes within the COF materials (Figure 2).

Therefore, upon excitation, the charge carriers photo-generated respectively at the VB(h^+) and CB(e^-) of COF can oxidize or reduce an electron donor (D) or an acceptor (A) substrate to form the corresponding radical cation ($D^{\bullet+}$) and radical anion ($A^{\bullet-}$) species.

This electron transfer event is favored ($\Delta G < 0$) if the redox potential of the couples $D^{\bullet+}/D$ and $A^{\bullet-}/A$ lie within those of

Table 1. Selection of COF-Based Photocatalysts for Light-Driven Organic Transformations

Building block 1	Building block 2	COF photocatalyst	Reaction type
Th	Th	CTF-Th@SBA-15 ³⁶	Alcohols oxidation
TPA	TAPB	NH ₂ -MIL-125 ³⁷ /TiO ₂ @COF ³⁸	
DBD	TFPT/TFP/TFPy	LZU-190/191/192 ³⁹	Arylboronic Acids Oxidation
BBO	BBO	BBO-COF ⁴⁰	
TFB	TAPB	COF-1a/b ⁴¹	Arylboronic Acids & Sulfides Oxidation
TPA	TAM	COF-1c ⁴¹	
<i>p</i> -PdPor-CHO	PPDA/TAM	2d/3d-PdPor-COF ⁴²	Sulfides Oxidation
TFB	TAPB	Pt@COF ⁴³	
TFB	PPDA	h-LZU1 ⁴⁴ and Pd/TiATA@LZU1 ⁴⁵	Sulfides Oxidation & Olefins reduction
<i>p</i> -PdPor-CHO	PDAN	Por-sp2c-COF ^{46, 47}	Amines Oxidation
BMTH	TFPT	TFPT-BMTH-COF ⁴⁸	
A	TFPB/TFPT	B-COF-2/T-COF-2 ⁴⁹	NADH regeneration
TFB	DMTH	TFB-COF ⁵⁰⁻⁵³	C-C and N-S formation
TTA	DMTP	COF-JLU5 ⁵⁴	C-C formation
X-TFP	TTA/TAPB	X-TFP-TTA/X-TFP-TAPB ⁵⁵	
NBC	ETTA	COF-1 ⁵⁶	
BADA	ETBC	COF-2 ⁵⁶	
BTDA	PyTTA	COF-JLU22 ⁵⁷	
BPDA	TMT	2D-COF-2 ⁵⁸	
Ace	TTA	Ace-COF ⁵⁹	
Mel	Tp	TpTt ⁶⁰	Isomerization

Building blocks structure

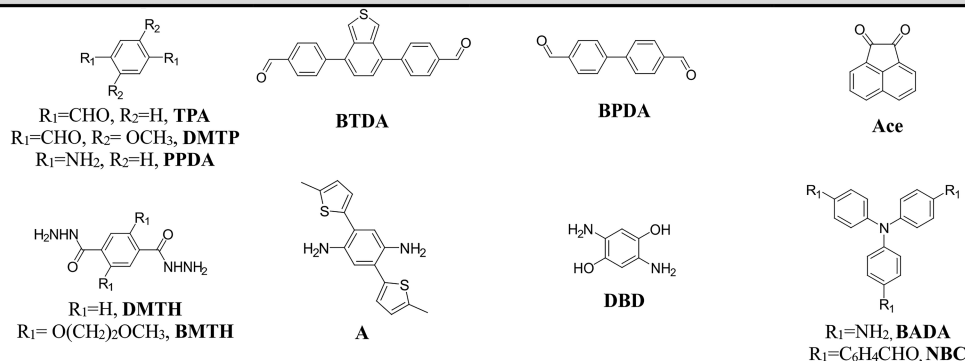


Table 1. continued

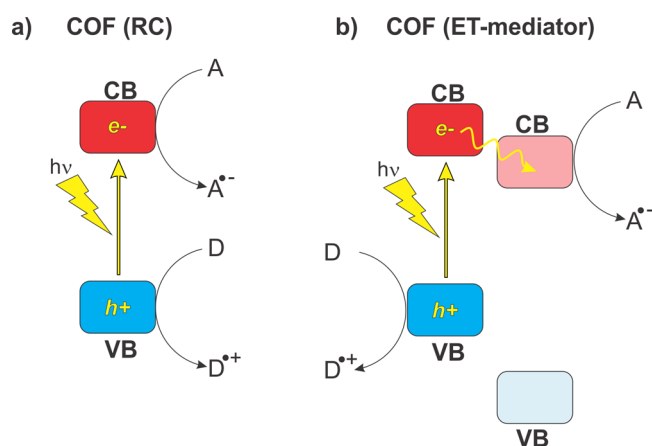
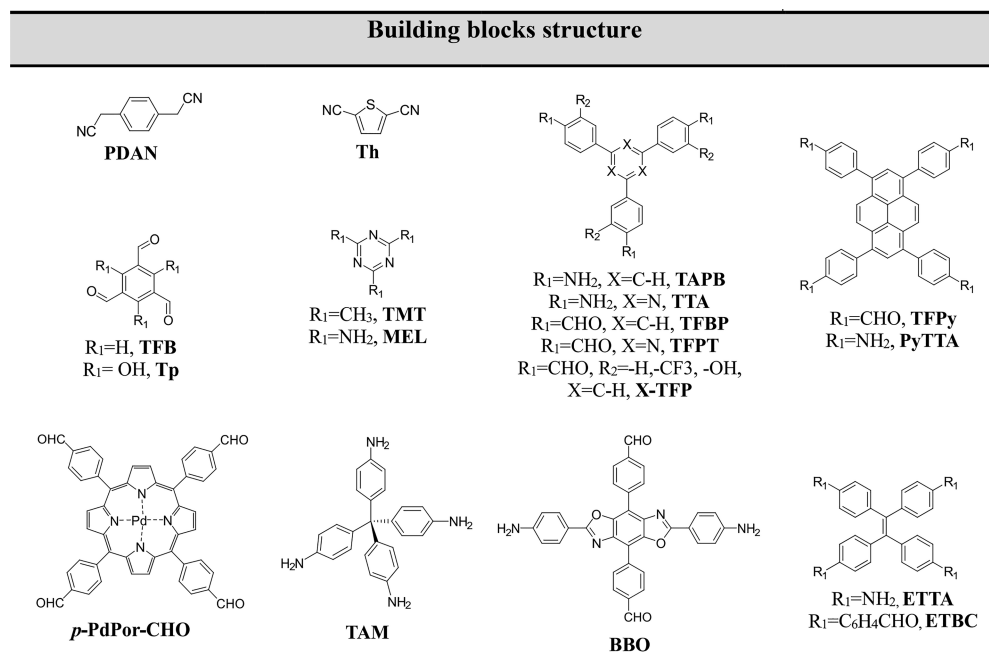


Figure 2. Schematic depiction of the electron transfer mechanism involved in COF-based photocatalyst. “A” and “D” stand for electron acceptor and donor species, while VB and CB refer to valence and conduction bands. “RC” and “ET” stand for reaction center and electron transfer, respectively.

the photogenerated charge carriers, that is, above and below the energy potential of VB and CB, respectively (Figure 2a). In this case, the COF photocatalyst acts as a reaction center (RC) where the photoinduced charge separation is developed and is directly responsible for productive redox events involving the substrate.

Otherwise, the excited COF can also act as an electron-transfer (ET) mediator when coupled with other materials (MOF, inorganic semiconductor, e.g., TiO_2 , metal domains). In this case, the photogenerated COF electrons/holes can be transferred at the interface between the two materials that display favorable energy gaps, and the productive steps involving the substrate follow this ET cascade and originates from the coupled materials. Figure 2b illustrates a COF ET mediator case, where, upon photoexcitation, electrons are injected from the COF-CB(e^-) into the interfaced material CB, which can act as the competent reduction site for the

substrate $A/A^{\bullet-}$ couple. These COF hybrids have the advantage of increasing the lifetime of the charge carriers, because of the charge transport across the interfacial heterojunction slowing recombination and being amenable to the use of sacrificial scavengers to restore the COF ground state (D in Figure 2b). Interestingly, COFs can also behave as light-harvesting (LH) units to trigger photocatalysis by ET mechanisms. Prominent examples of photoinduced COF ET have been reported in the case of singlet oxygen generation ($^1\text{O}_2$) and in the visible light isomerization of *E/Z* olefins, where, in both cases, energy transfer from a photogenerated COF triplet state (T_1) is invoked.⁶¹ It turns out that the choice of photoactive building blocks and linkers can have a huge impact on the photocatalytic mechanism of the resulting COF. Tuning of the band gap, as well as the relative stabilization of the COF excited states, gives access to a rich mechanistic spectrum at the crossroad between molecular and materials behavior. This multifaceted photocatalytic behavior lies at the origin of the high potential that COFs display in photochemical reactions, as highlighted in the next sections for diverse functional group transformations.

Oxidation Reactions. Selective oxidation of both aliphatic and aromatic compounds is one of the fundamental reactions in industrial processes to produce fine chemicals. Harsh conditions are generally employed, including high temperature and hazardous oxidizing agents (permanganate and dichromate among others), raising operative costs and undesired products, as well as a severe environmental impact. COF-based photocatalysis under aerobic conditions can play a key role in contrasting the “collateral effects” of these traditional oxidation methods, since the combination of sunlight and molecular oxygen are the desired reagents for a transition to sustainable and green synthetic methods.

Below are some remarkable examples where COFs have been employed as photocatalysts in the oxidation reactions, specifically in the oxidative transformation of alcohols, boronic acids, sulfides, and amines. All the reactions mentioned above share a common mechanism, that is, upon COF excitation,

Scheme 1. (a) Schematic Illustration of the Synthesis of CTF-Th@SBA-15 Material. [Reprinted with permission from ref 36. Copyright 2017, American Chemical Society, Washington, DC.] (b) CTF-Th@SBA-15 Application in Photo-oxidation of Aryl Alcohols

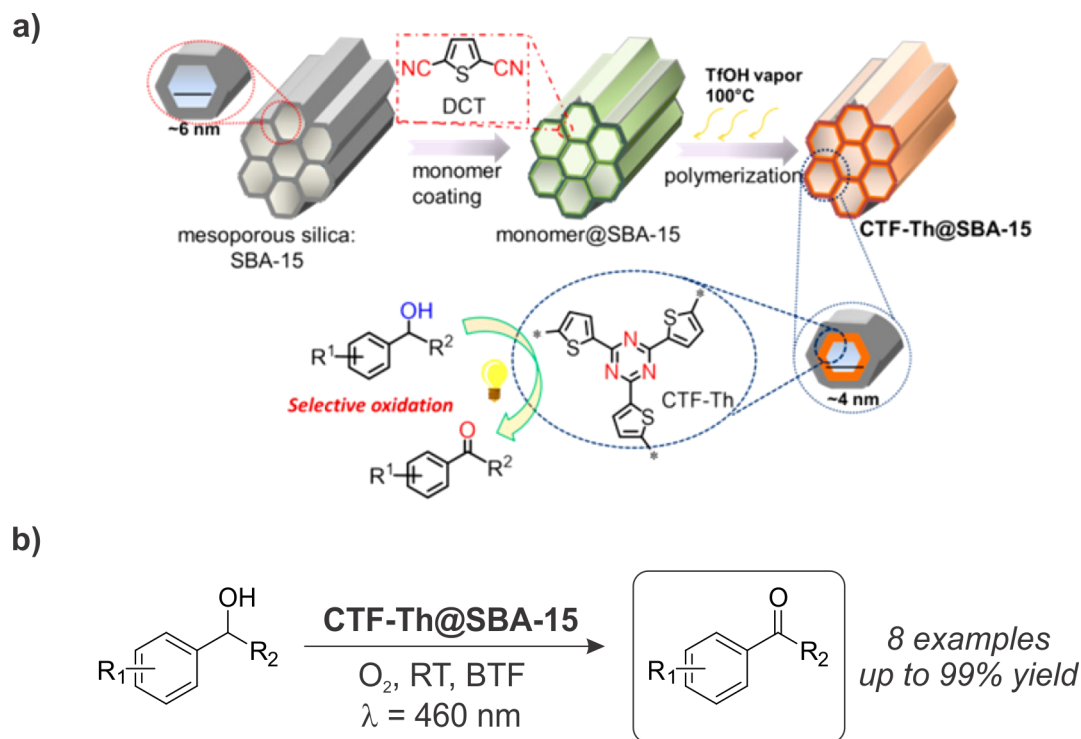


Table 2. Comparison of the Catalytic Performance of COFs in the Photo-oxidation of Benzyl Alcohol

COF system (entry)	COF building blocks	VB/CB (V vs SCE)	yield, t_R	solvent	light source, E_e (W/m^2)
CTF-Th@SBA-15 (i)	DCT	+1.75/−0.72	>99% (4 h)	BTF	$\lambda = 460$ nm, LED, (0.16)
TiO ₂ @COF-3 (ii)	TAPB, TPA	+2.09/−0.73	>93% (30 h)	CH ₃ CN	$\lambda = 420$ –780 nm, LED (0.15)
NH ₂ -MIL-125@COF (iii)	TAPB, TPA	+2.09/−0.73	>93% (30 h)	CH ₃ CN	$\lambda = 420$ –780 nm, LED, (0.15)

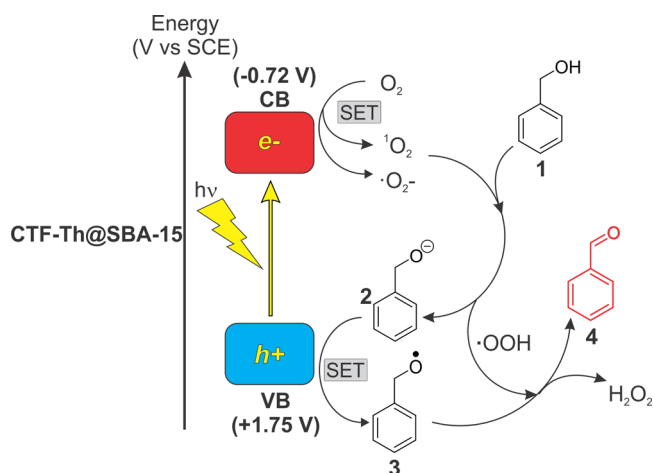
^aAbbreviations used: DCT = 2,5-dicyanothiophene, TAPB = 1,3,5-tris(4-aminophenyl)benzene, TPA = terephthaldehyde, t_R = reaction time, E_e = irradiance flux density, BTF = benzotrifluoride.

molecular oxygen is converted either to singlet oxygen (energy transfer) and/or to superoxide radical anion (electron transfer). Photogenerated holes at the COF VB are scavenged by either the desired substrates (e.g., sulfides) or by sacrificial electron donors (e.g., tertiary amines). Importantly, in the case of the electron transfer mechanism, COF must have a suitable thermodynamic driving force to power the photo-oxidation reactions, that is, the energy potential of the COF CB must be lower than the redox potential of the couple $O_2^{\bullet-}/O_2$ ($E^\circ = -0.56$ V vs SCE), while the energy potential of the COF VB must be higher than the redox potential of the substrate of interest.

Alcohol Oxidation. A thiophene-covalent triazine framework, CTF-Th, has been employed for the first time in 2017 by Zhang et al. for visible-light photo-oxidation of aryl alcohols (see Scheme 1b, and Table 2, entry (i)).³⁶ Elegantly, CTF-Th was incorporated onto silica SBA-15 to obtain a mesoporous nanoreactor CTF-Th@SBA-15, as revealed by SEM and HR-TEM spectroscopy showing cylinder morphology with 2D hexagonal channels (Scheme 1a). UV–vis diffuse reflectance

spectrum of CTF-Th@SBA-15 displays a broad absorption up to ca. 520 nm corresponding to a band gap of 2.47 eV, while the VB and CB have been determined by cyclic voltammetry to be +1.75 and −0.72 V vs SCE, indicating the relatively high oxidizing and reducing nature of CTF-Th@SBA-15.

The reaction mechanism depicted in Scheme 2 has been proposed on the basis of several control experiments. Blue light irradiation ($\lambda = 460$ nm) triggers, at the CTF-Th@SBA-15 VB, the oxidation of alkoxide 2 to the corresponding radical 3, while the reduction of O_2 into superoxide radical anion ($E^\circ(O_2^{\bullet-}/O_2) = -0.56$ V vs SCE) occurs at the CTF-Th@SBA-15 CB. Both these oxidation and reduction processes occur by a single electron transfer mechanism (SET). The presence of singlet oxygen has also been proved by the authors employing NaN_3 as O_2^1 scavenger, indicating that the photoreduction of molecular oxygen is also occurring via an energy transfer mechanism concurrently with the formation of $O_2^{\bullet-}$ species. The corresponding aldehyde 4 is then formed by the reaction between alkoxy radical 3 and the hydroperoxy radical ($HOO\cdot$), the latter species generated via proton

Scheme 2. Mechanism for Benzyl Alcohol Oxidation under Visible-Light Irradiation Catalyzed by CTF-Th@SBA-15^a


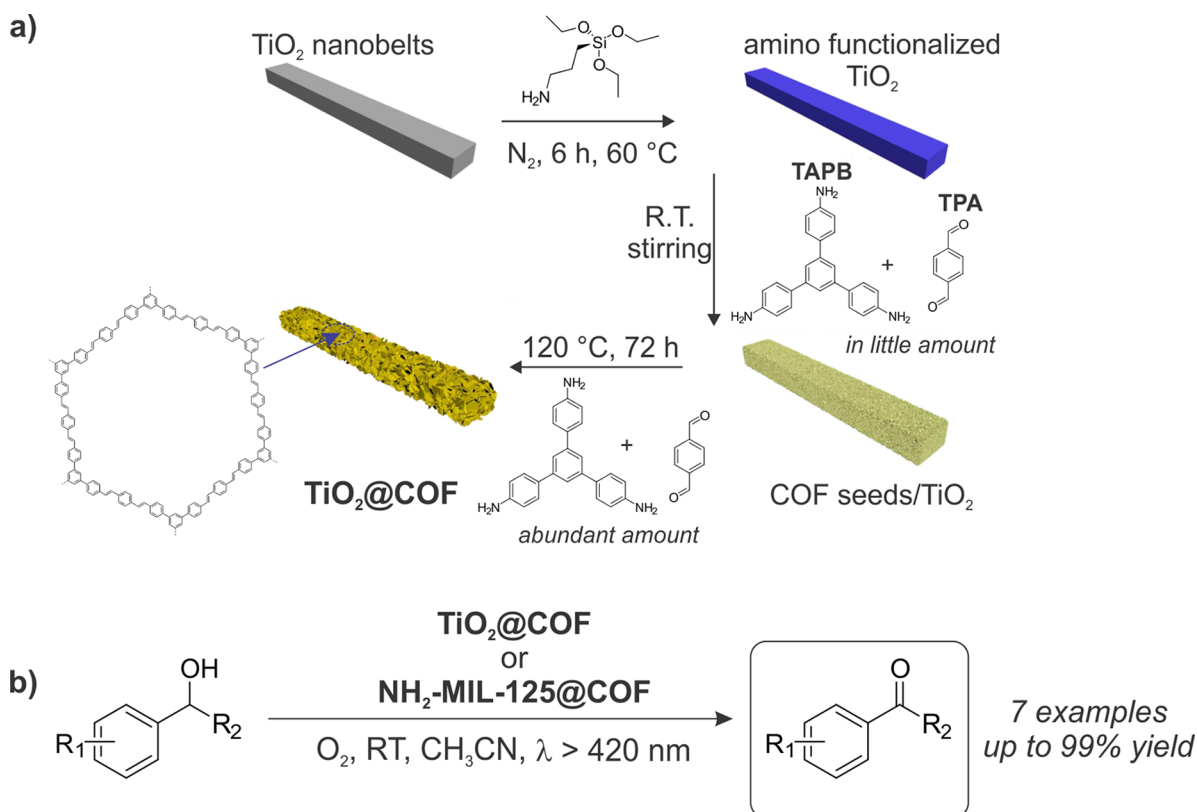
^aAdapted with permission from ref 36. Copyright 2017, American Chemical Society, Washington, DC.

abstraction from the starting alcohol **1** by superoxide radical anion species, yielding H₂O₂ as a side product. Importantly, CTF-Th@SBA-15 proved to be an excellent heterogeneous photocatalyst, since it did not show any remarkable loss of catalytic activity after five sequential reaction cycles without any evidence of structural degradation.

Aerobic visible-light ($\lambda > 420$ nm) photo-oxidation of alcohols has also been successfully performed employing hybrid COF materials as heterogeneous photocatalysts by the group of Wang et al. in 2019 (see Scheme 3b, as well as Table 2, entries (ii) and (iii)).^{37,38} TiO₂ nanobelts have been coated with a COF solid, produced by condensation reaction between terephthalaldehyde (TPA) and 1,3,5-tris(4-aminophenyl)benzene (TAPB), employing a novel seeding growth technique to yield TiO₂@COF composites as core-shell structures (Scheme 3a).

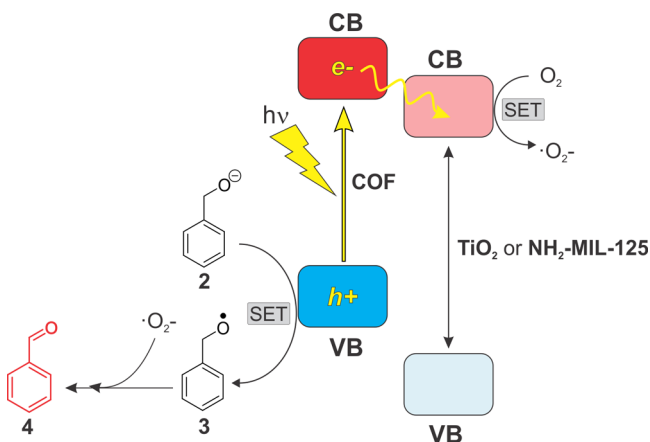
Using a similar approach, the nanocomposites NH₂-MIL-125@COF have been fabricated replacing the TiO₂ nanobelts with the MOF (MIL-125) functionalized with amino groups. Both composites, TiO₂@COF and NH₂-MIL-125@COF, showed a broad absorption up to ca. 500 nm, corresponding to a band gap of ~ 2.7 eV, while displaying remarkable photocatalytic activity and selectivity toward the oxidation of aryl alcohols. Control experiments demonstrated that pure TiO₂, NH₂-MIL-125, and COF, tested separately, yielded negligible product yield under the same conditions. Such performance increase in the hybrid materials has been attributed to the reduced probability of the charge-carrier recombination, as shown through a careful set of analyses, including transient photocurrent response, electrochemical impedance spectroscopy, and photoluminescence quenching measurements.

The reaction mechanism depicted in Scheme 4 has been proposed by the authors, where the COF is acting as an ET mediator by depositing the photogenerated electrons in the TiO₂/NH₂-MIL-125 CB. Thus, the photo-oxidation process of

Scheme 3. (a) Seeding Growth Strategy To Obtain TiO₂@COF Composites.^a (b) TiO₂@COF and NH₂-MIL-125@COF Application in Photo-oxidation of Aryl Alcohols


^aAdapted with permission from ref 38. Copyright 2019, Elsevier.

Scheme 4. Mechanism for the Benzyl Alcohol Oxidation under Visible-Light Irradiation Catalyzed by TiO₂@COF or NH₂-MIL-125@COF^a



^aAdapted with permission from refs 37 (Copyright 2019, Elsevier) and 38 (Copyright 2020, Elsevier).

benzyl alcohol occurs similarly to the mechanism shown in Scheme 2 with the difference being that the oxygen reduction ($E^\circ(\text{O}_2^{\bullet-}/\text{O}_2) = -0.56 \text{ V vs SCE}$) is occurring at the conduction band of the interfaced material (TiO₂@COF CB/NH₂-MIL-125@COF CB, $E = -0.73 \text{ V vs SCE}$) rather than in the COF CB. Unfortunately, no experiments have been performed by the authors to exclude the generation of singlet oxygen during the photo-oxidation process. Both TiO₂@COF and NH₂-MIL-125@COF displayed excellent stability retaining a similar catalytic activity and selectivity over five reaction cycles showing great potential as heterogeneous photocatalysts.

Oxidation of Arylboronic Acids. COF materials also proved to be high-performant photocatalysts in oxidative hydroxylation of arylboronic acids to phenols, as shown by a recent work of Wang and co-workers (see Scheme 5b, and Table 3, entry (i)).³⁹ Three novel COFs—LZU-190, LZU-

191, and LZU-192—have been prepared under solvothermal conditions via the condensation of 2,5-diamino-1,4-benzenediol dihydrochloride (DBD) with three different aldehyde building blocks, such as 1,3,5-triformylbenzene (TFB), 2,4,6-tris(4-formylphenyl)-1,3,5-triazine (TFPT), and 1,3,6,8-tetrakis(4-formylphenyl)pyrene (TFPy), respectively. The LZU-COFs are characterized by the formation of benzoxazole ring, following a mortise-and-tenon model, resulting in exceptional photocatalyst properties (Scheme 5a): (i) persistent chemical stability in a wide pH range (from HCl, 9M to NaOH, 9M), (ii) excellent photostability as no sign of structure degradation is observed upon 3 days of continuous exposure to visible light, and (iii) extended optical absorption to NIR region (up to 900 nm), corresponding to a band gap in the range between 2 eV and 2.4 eV.

The photo-oxidation of arylboronic acid 4 is believed to proceed via the addition of superoxide radical anion, generated via single electron transfer (SET) from the LZU-COF CB, to form the boron intermediate 6, which abstract a hydrogen from *i*Pr₂NEt radical cation to give 7. Subsequent rearrangement and hydrolysis yield the final product 8 (Scheme 6). The photocatalytic cycle is then generally completed by a sacrificial agent (*i*Pr₂NEt), even though LZU-190 displayed photocatalytic activity, even in the absence of *i*Pr₂NEt suggesting that the terminal amino groups of the framework act as electron donor species. However, the latter pathway is not yet well-understood. Most importantly, LZU-190 displayed unprecedented recyclability since the catalytic activity remains unvaried even after 20 reaction runs without crystallinity and morphology loss of the recycled material. Notably, Wang et al. also explored the size-selective effect of LZU-190, showing that the reaction yields decreased as the size of the substrate increased. For instance, the lowest yield has been observed when using 1-pyrenylboronic acid (1.2 nm × 0.9 nm) as substrate, whose size is comparable to the LZU-190 pore width (1.4 nm), suggesting that the lower photoconversion stems from the poor absorption of the substrate within the porous COF structure (size selectivity).

Scheme 5. (a) Synthesis of LZU-190 by Benzoxazole Ring Formation (Mortise-and-Tenon Model). (b) LZU-190 Application in Photo-oxidation of Aryl Boronic Acids

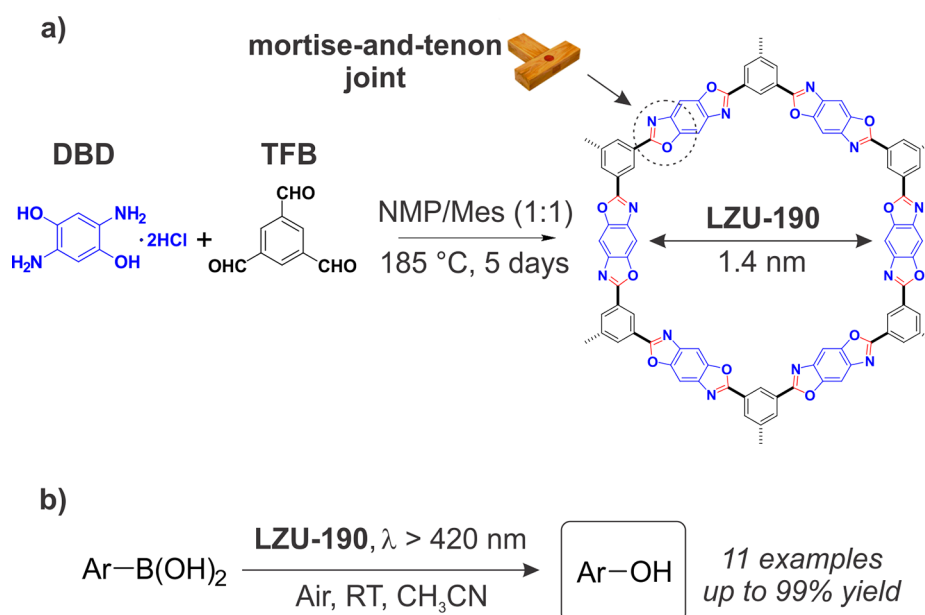

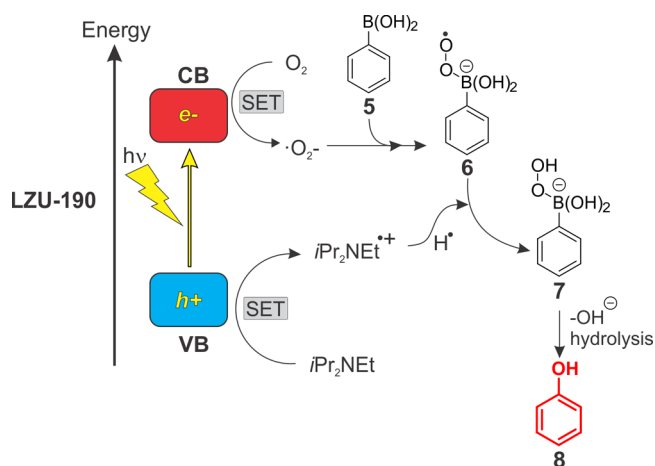


Table 3. Comparison of the Catalytic Performance of COFs in the Photo-oxidation of Phenyl Boronic Acid^a


COF name (entry)	COF building blocks	band gap (eV)	yield, t_R	solvent	light source (power)
LZU-190 ^b (i)	TFB, DBD	2.02	88% (72 h)	CH ₃ CN	white light (LED, 20 W)
BBO-COF ^c (ii)	BBO	2.24	99% (96 h)	CH ₃ CN/H ₂ O	white light (LED, 18 W)
COF-1a ^d (iii)	TAPB, TFB	2.85	59% (72 h)	EtOH/H ₂ O	$\lambda = 450$ nm (LED, 15 W)
COF-1b ^d (iv)	TAPB, TFB	2.90	72% (72 h)	EtOH/H ₂ O	$\lambda = 450$ nm (LED, 15 W)
COF-1c ^d (v)	TAM, TPA	2.53	40% (72 h)	EtOH/H ₂ O	$\lambda = 450$ nm (LED, 15 W)

^aAbbreviations used: TFB = 1,3,5-triformylbenzene, DBD = 2,5-diamino-1,4-benzenedioldihydrochloride, BBO = 4,4'-(2,6-bis(4-aminophenyl)-benzo[1,2-*d*:4,5-*d'*]bis(oxazole)dibenzaldehyde, TAPB = 1,3,5-tris(4-aminophenyl)benzene, TAM = tetra(4-anilylmethane), TPA = terephthalaldehyde, t_R = reaction time, ^b*i*Pr₂NEt as SED. ^cDIPEA as SED. ^dEt₃N as SED.

Scheme 6. Mechanism for the Aryl Boronic Acids Oxidation under Visible-Light Irradiation Catalyzed by LZU-190^a



^aAdapted with permission from ref 39. Copyright 2018, American Chemical Society, Washington, DC.

Oxidation of arylboronic acids has also been investigated by Chen and co-workers, where they employed a “two-in-one” strategy to produce an ultrastable imine-based COF, BBO-COF, acting as a photocatalyst (Table 3, entry (ii)).⁴⁰ The key design in this approach relies on the self-condensation of a bifunctional monomer carrying two formyl and two amino groups in a single benzoxazole ring. BBO-COF showed higher chemical and thermal stability, compared to most reported imine-linked COF making it a high-performance heterogeneous photocatalyst, as reflected by its structural retention, even after 10 runs of cyclic reactions.

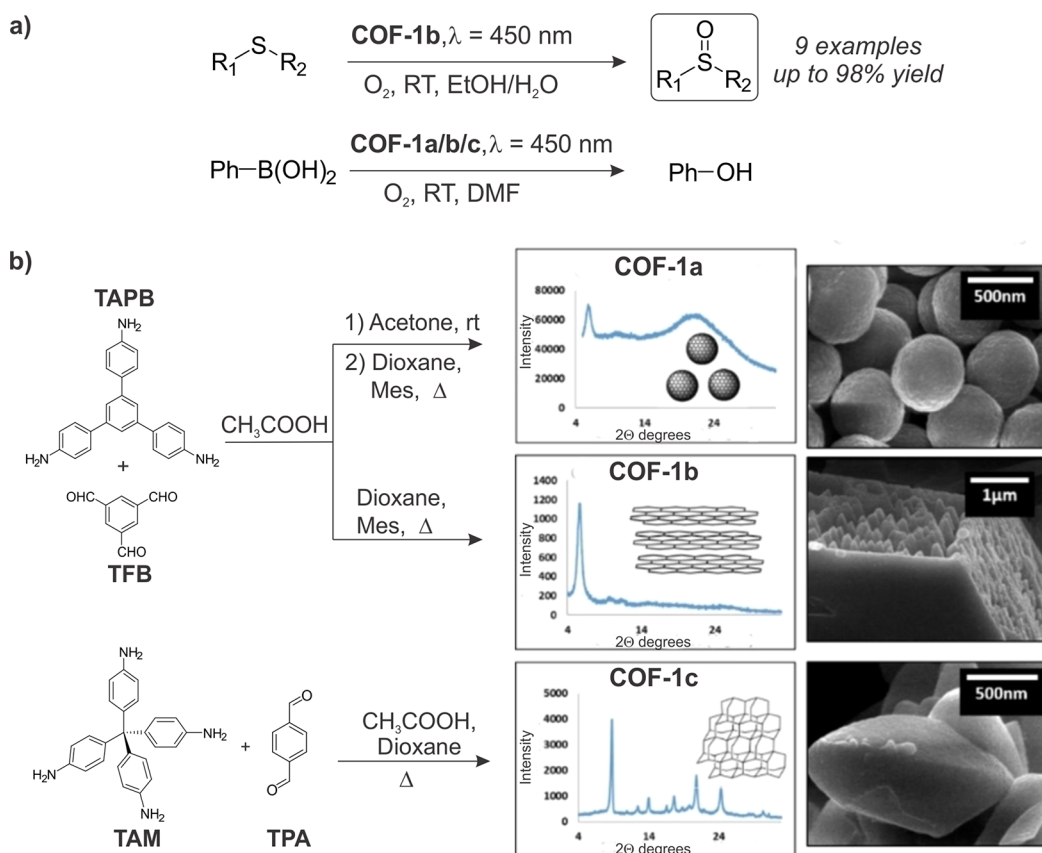
In an elegant study, Aleman et al. examined the photo-oxidation of phenyl boronic acid (see Scheme 7a, and Table 3, entries (iii)–(v)) and photosulfoxidation (see Scheme 7a, and Table 4, entries (vii)–(ix)) reactions employing imine-based COFs with laminar (COF-1a), spherical (COF-1b), and 3D (COF-1c) structures either in crystalline (Scheme 7b) and amorphous phase.⁴¹ Diffuse reflectance spectra of the as-prepared COFs displayed absorbance with maximums ranging from 430 nm to 475 nm corresponding to band gap values of 2.8, 2.5, and 2.7 eV for COF-1a, COF-1b, and COF-1c respectively. Similar values of band gap have been found between amorphous and crystalline COFs. A comparison of the COFs catalytic activity vis-à-vis their crystallinity phase has also been examined. It has been shown that in all cases crystalline materials performed better than the corresponding

amorphous counterpart except for the 3D structure. Among the crystalline COFs, the lamellar system is the one with higher performance (Table 3, entry (iv)).

Oxidation of Sulfides. COF-based photocatalysts have also been successfully employed for the selective oxidation of sulfides to sulfoxides. A notable example is the recent work of Wang et al., where the authors investigated the photocatalytic performance as a function of COF dimensionality.⁴² They prepared and characterized 2D and 3D palladium porphyrin-based COFs (2D-PdPor-COF and 3D-PdPor-COF) and tested them as heterogeneous photocatalysts in the oxidation of aromatic sulfides (Schemes 8a and 8b).

The proposed reaction mechanism is depicted in Scheme 9. The triplet state of 2D/3D-PdPor-COF is generated upon blue-light irradiation and the electron promoted at the COF-CB reduces molecular oxygen to O₂^{•-} species. Concurrently, the photogenerated holes at the COF-VB oxidize sulfide 9 to the corresponding radical cation 10, which, in turn, reacts with the superoxide radical anion to yield the desired product 11. No experiments have been performed to confirm the generation of O₂¹ during the photochemical process, even though Aleman et al., employing COF-1a/b/c as photocatalysts for a similar reaction, showed that the singlet oxygen is produced, along with O₂^{•-} species.⁴¹ 3D-PdPor-COF displayed better photocatalytic activity, reaching 99% yield in the conversion of 4-methylthioanisole to the corresponding sulfoxide in 24 min under blue-light irradiation (Table 4, entry (ii)) while employing 2D-PdPor-COF the product yield decreased to 60% (Table 4, entry (i)).

In order to understand the reason why the catalytic performance between 2D-PdPor-COF and 3D-PdPor-COF differs, the authors studied the triplet lifetime of both COFs using transient absorption spectroscopy. 2D-PdPor-COF displayed a shorter lifetime (0.41 μs) than 3D-PdPor-COF (26.34 μs) which is consistent with their crystal structure. Indeed, in 2D-PdPor-COF, the porphyrin building blocks are closer to each other, compared to the 3D-PdPor-COF (Scheme 8a), which induces a major self-quenching of the photoluminescence emission resulting in a shorter triplet lifetime. Consequently, under the same conditions, the generation of superoxide radical anion by photoinduced ET is less efficient, because of the limited lifetime of the COF excited state. Noteworthy, 3D-PdPor-COF, which features smaller pores (0.58 nm) than 2D-PdPor-COF (1.9 nm), displayed interesting confinement effects (size-selective photo-reactivity), since the reaction yields decreased when substrates with larger sizes (dimensions up to 0.9 nm × 0.5 nm) have

Scheme 7. (a) COFs 1a–1c Application in Photo-Oxidation of Sulfides and Phenyl Boronic Acid. (b) Solvothermal Conditions for the Synthesis of Crystalline Imine-COFs 1a–1c and Powder XRD Analysis of the Crystalline Materials^a

^aModified with permission from ref 41. Copyright 2019, Wiley–VCH GmbH.

Table 4. Comparison of the Catalytic Performance of the COFs in the Photo-oxidation of 4-Methylthioanisole

COF name (entry)	COF building blocks	band gap (eV)	yield, t_R	solvent	light source (power)
2D-PdPor-COF (i)	<i>p</i> -PdPor-CHO, PPDA	/	60% ^a (0.4 h)	CF ₃ CH ₂ OH	blue LED (3 W)
3D-PdPor-COF (ii)	<i>p</i> -PdPor-CHO, TAM	/	99% ^a (0.4 h)	CF ₃ CH ₂ OH	blue LED (3 W)
Pt@COF (iii)	TAPB, TFB + truncated TAPB monomer	/	88% (7 h)	CH ₃ OH	$\lambda = 450 \text{ nm}$ (LED, 15 W)
Pt@COF-Annealed (iv)	TAPB, TFB + truncated TAPB monomer	/	75% (7 h)	CH ₃ OH	$\lambda = 450 \text{ nm}$ (LED, 15 W)
COF (v)	TAPB, TFB	/	10% (7 h)	CH ₃ OH	$\lambda = 450 \text{ nm}$ (LED, 15 W)
COF-Annealed (vi)	TAPB, TFB	/	33% (7 h)	CH ₃ OH	$\lambda = 450 \text{ nm}$ (LED, 15 W)
COF-1a (vii)	TAPB, TFB	2.85	100% (24 h)	EtOH/H ₂ O	$\lambda = 450 \text{ nm}$ (LED, 15 W)
COF-1b (viii)	TAPB, TFB	2.90	100% (24 h)	EtOH/H ₂ O	$\lambda = 450 \text{ nm}$ (LED, 15 W)
COF-1c (ix)	TAM, TFB	2.53	69% (24 h)	EtOH/H ₂ O	$\lambda = 450 \text{ nm}$ (LED, 15 W)
h-LZU1 ^a (x)	ZIF8, ^a TFB, PPDA	2.71	100% (22 h)	CH ₃ CN	$\lambda > 380 \text{ nm}$ (300 W, Xe lamp)

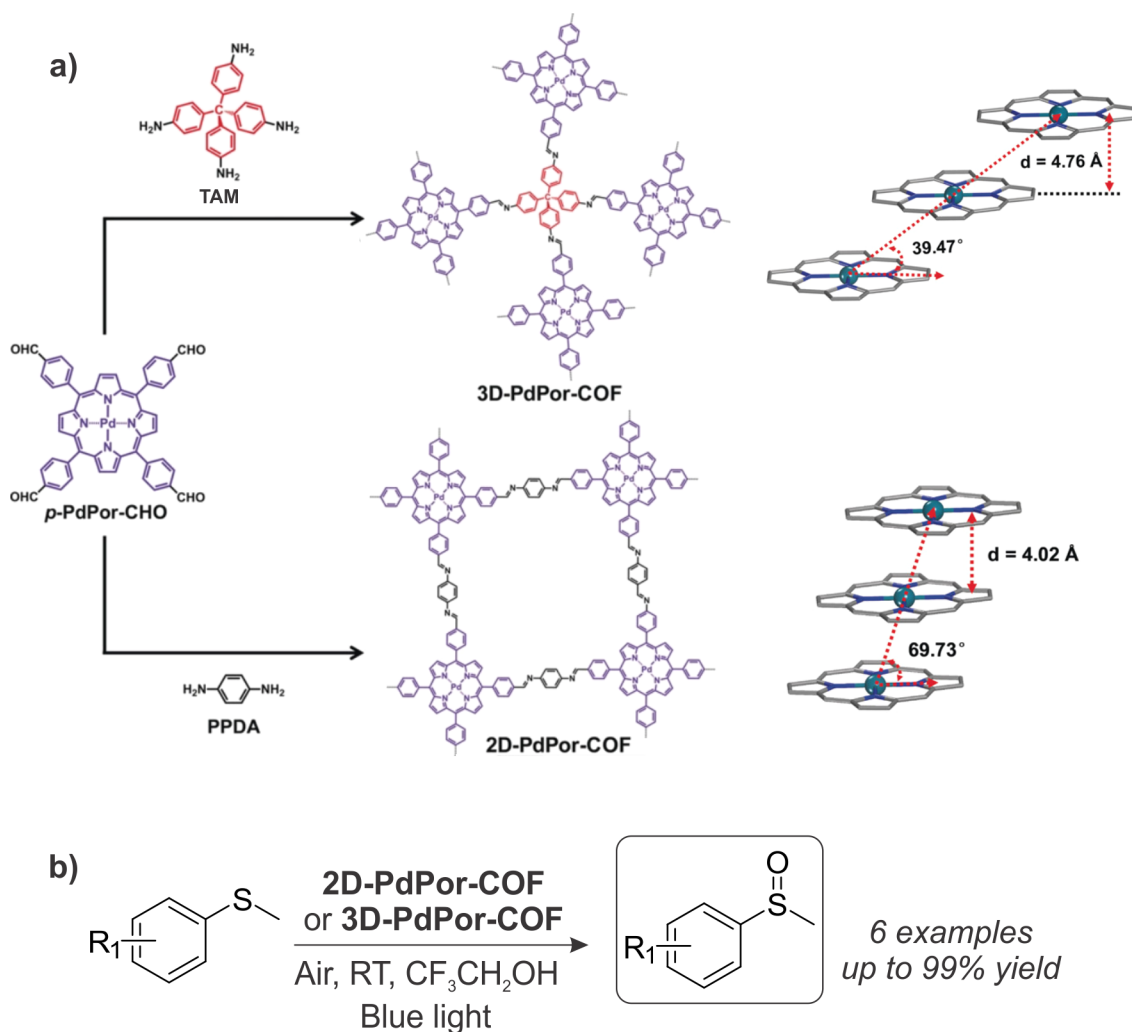
^aReaction performed under air. ^bMOF used as template, t_R = reaction time, *p*-PdPor-CHO = [5,10,15,20-tetrakis(4-benzaldehyde)porphyrin]-palladium, PPDA = *p*-phenylenediamine, TAPB = 1,3,5-tris(4-aminophenyl)benzene, TAM = tetra(4-anilylmethane), TPA = terephthaldehyde, TFB = 1,3,5-triformylbenzene.

been tested. Importantly, 3D-PdPor-COF retained a similar catalytic activity, even after three reaction runs, fully retaining its framework.

Recently, Aleman et al. incorporated a Pt(II)-hydroxyquinoline complex **12** into a 2D layered COF framework through a monomer truncation strategy, which consists of blocking a linking point of one of the building blocks (Scheme 10a).⁴³ Notably, a low crystalline material (Pt@COF) and a higher-

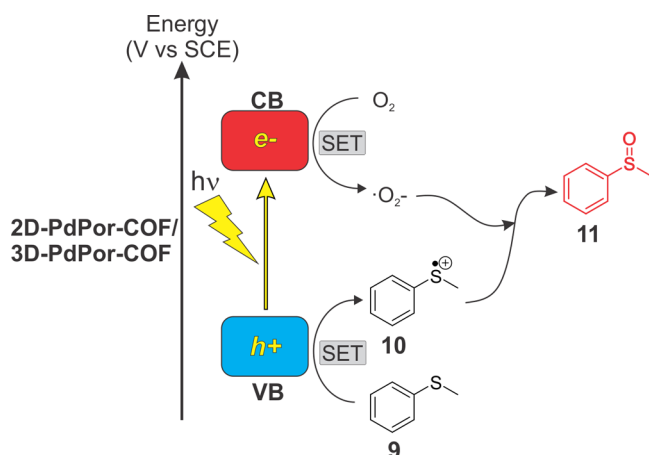
order material (Pt@COF-Annealed) have been prepared. Then, Aleman and co-workers compared the photocatalytic activity of Pt@COF and Pt@COF-Annealed in the photo-sulfoxidation reaction (Scheme 10b) with untruncated COFs both in their crystalline (COF-Annealed) and amorphous phase. Interestingly, COF-Annealed performed better than the amorphous polymer (see Table 4, entries (v) and (vi), respectively), probably because of the extended conjugation

Scheme 8. (a) Synthesis of 3D-PdPor-COF and 2D-PdPor-COF with the Corresponding Stacking Configuration.^a (b) 2D/3D-PdPor-COFs Application in Photo-oxidation of Sulfides



^aModified with permission from ref 42. Copyright 2019, Wiley–VCH GmbH.

Scheme 9. Mechanism for Photo-oxidation of Aryl Sulfide Catalyzed by 2D/3D-PdPor-COFs^a

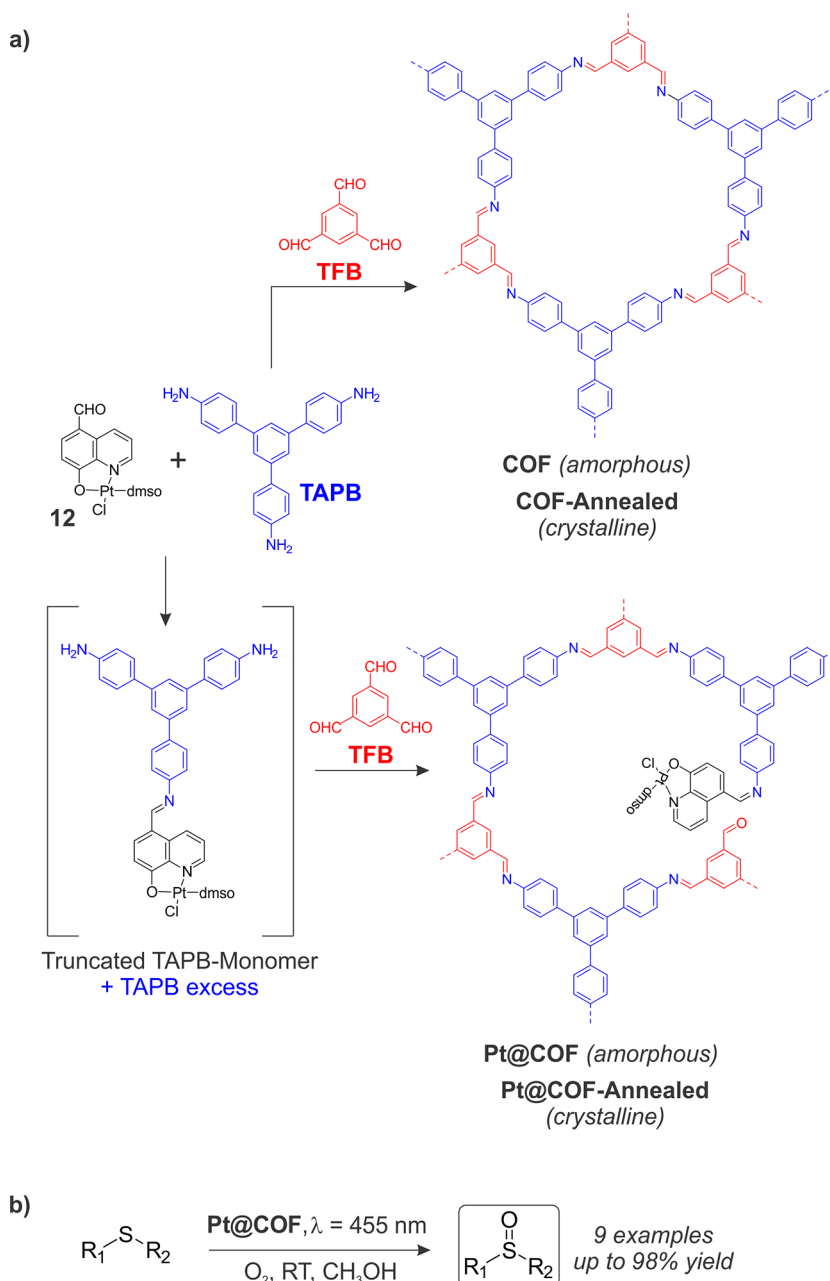


^aAdapted with permission from ref 42. Copyright 2019, Wiley–VCH GmbH.

across the crystalline material. Incorporation of the Pt(II)-hydroxyquinoline complex leads to a remarkable increase of the product yield, more than double, compared to both untruncated COFs (Table 4, entries (iii) and (iv), respectively). However, Pt@COF and Pt@COF-Annealed do not follow the same trend as that seen in their untruncated COF counterparts, that is, an increase of crystallinity does not correspond to a higher product yield (Table 4, entries (iii) and (iv), respectively). Probably, as the authors suggested, the photocatalytic activity of Pt@COF and Pt@COF-Annealed is mainly regulated by the Pt-active sites, while the overall material plays a minor role. Importantly, Pt@COF proved to be a robust heterogeneous photocatalyst maintaining its structure after several 8-h reaction cycles while detailed control tests discarded Pt leaching, indicating that the observed catalytic activity is only attributed to the Pt@COF material.

Photosulfoxidation has also been tested recently by Zhang using a novel COF capsule, h-LZU1, as light-harvesting material (Scheme 11b, Table 4 - entry (x)).⁴⁴ A MOF template route assisted by compressed CO₂ has been employed by the authors to construct h-LZU1 in a hollow waxberry-like structure with orderly assembled nanorods on the surface

Scheme 10. (a) Monomer Truncation Strategy for the Preparation of Pt@COF. (b) Pt@COF Application in Photo-oxidation of Sulfides



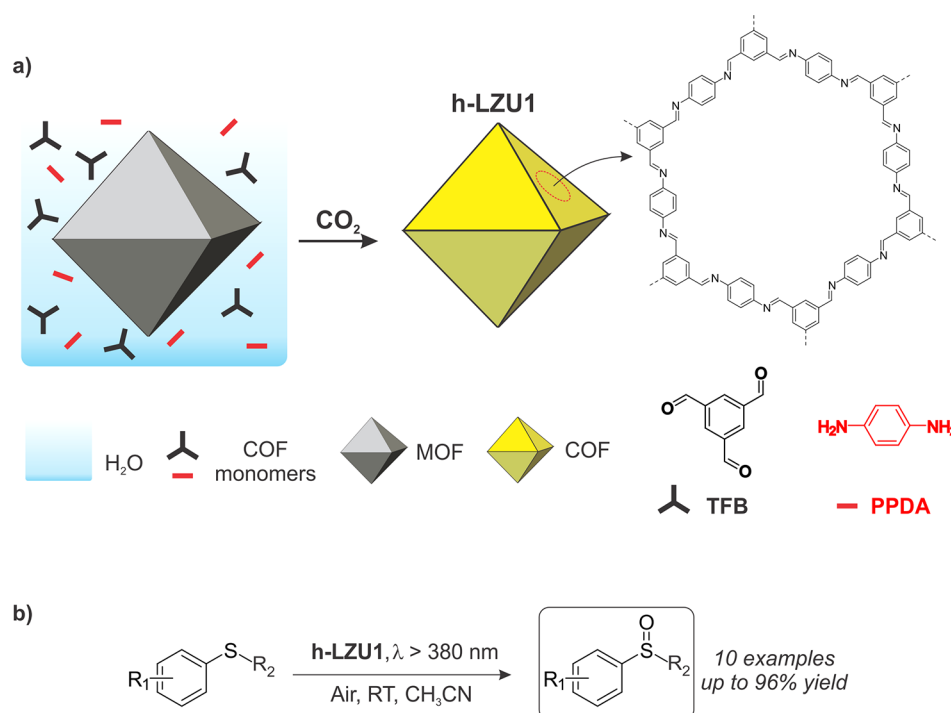
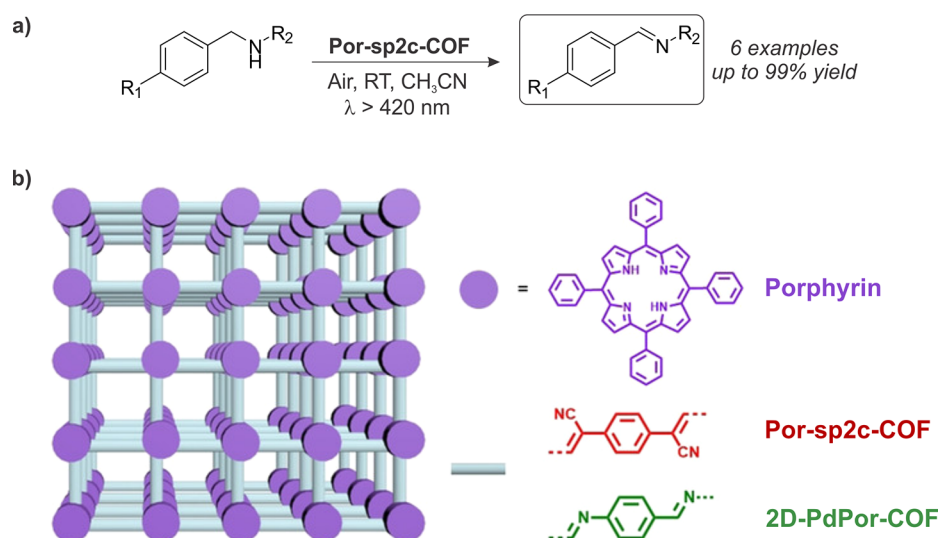
(Scheme 11a), which displayed a broad absorption up to ca. 500 nm, corresponding to a band gap of 2.71 eV.

Comparison between the photocatalytic activity toward visible-light oxidation of thioanisole derivatives of LZU1, obtained by classical solvothermal synthesis, and h-LZU1 showed that the latter has a better catalytic performance. The authors attributed this superior activity to the more negative potential of h-LZU1's CB (−0.72 V vs NHE) than that of LZU1 (−0.52 V vs NHE), which boosts the reduction of O₂ to ·O₂[−] radical, the latter species responsible for the oxidation of sulfide substrates. Unfortunately, no experimental results regarding the reusability of the photocatalyst have been presented in this case.

Amine Oxidation. A high chemically stable COF, Por-sp2c-COF, fully sp² carbon conjugated, has been recently prepared through Knoevenagel condensation reaction by Wang

and co-workers (Scheme 12b) and successfully tested as a heterogeneous photocatalyst in the visible-light aerobic oxidation of amines (Scheme 12a).⁴⁶ Por-sp2c-COF displayed higher catalytic activity than its imine-based COF homologue, 2D-PdPor-COF, which indicates that the carbon conjugated framework efficiently stabilizes the charge carrier and, thus, facilitates the ET processes. Indeed, in the diffuse reflectance spectra which feature a broad absorption up to ca. 750 nm for both COFs, the Soret band of Por-sp2c-COF is red-shifted ~30 nm, compared to that of 2D-PdPor-COF. These results further indicate that the π–π conjugation is more extended across the crystalline framework of Por-sp2c-COF, compared to 2D-PdPor-COF. Importantly, Por-sp2c-COF could also well catalyze the photo-oxidation of benzylamine to *N*-benzylidenebenzylamine (Table S, entry (i)), which is

Scheme 11. (a) Synthetic Strategy for the Synthesis of COF Capsule h-LZU1. (b) h-LZU1 Application in Photo-oxidation of Sulfides

Scheme 12. (a) Por-sp2c-COF Application in the Photo-Oxidation of Amines. (b) Schematic Structure of the High Chemically Stable Por-sp2c-COF and the Imine-Based 2D-PdPor-COF^a

^aModified from ref 47. Copyright 2020, Wiley-VCH GmbH.


something not feasible with imine-based COFs, because of their decomposition when in contact with primary amines.

In subsequent work, the same group explored the cooperative photocatalysis of Por-sp2c-COF with the (2,2,6,6-tetramethylpiperidin-1-yl)oxyl (TEMPO) in the photo-oxidation of primary and secondary amines using red light ($\lambda = 623 \text{ nm}$) over a wide substrate scope (Scheme 13a).⁴⁷ A detailed mechanistic investigation has been performed by the authors through kinetic studies, quenching experiments, and spin trapping agents, which are consistent with the photo-oxidation process depicted in Scheme 13b. Upon irradiation with red light, the electrons promoted in the

Por-sp2c-COF CB reduce molecular oxygen to its radical anion, which, in turn, abstracts hydrogen from TEMPO-H 15 forming H_2O_2 as a side product and restoring 13. TEMPO 13 is concomitantly oxidized to 14 by the photogenerated hole in the Por-sp2c-COF-VB. The TEMPO⁺ 14 is responsible to convert benzylamine 16 to benzylideneamine 17, which further react with 16 to yield the targeted imine product 18 (Scheme 13b).

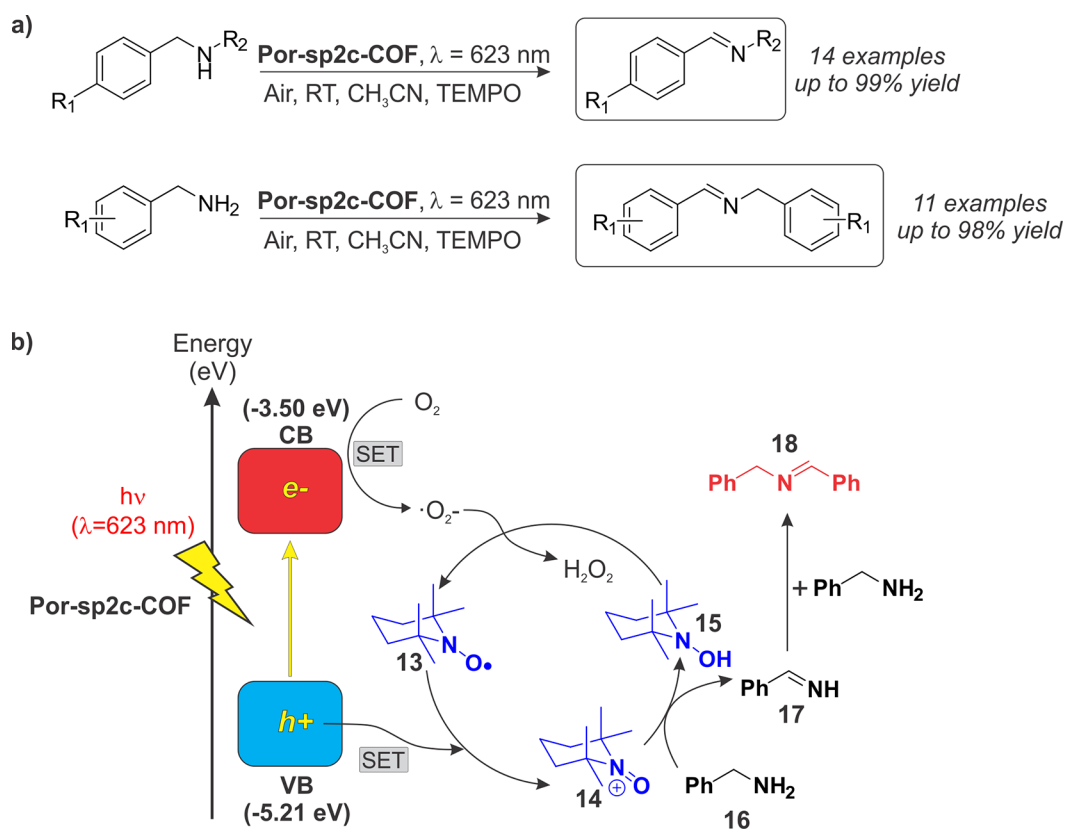
The cooperation mechanism involving TEMPO and Por-sp2c-COF has been assessed by cyclic voltammetry (CV) experiments. The intensity of the one oxidation peak recorded

Table 5. Comparison of the Catalytic Performance of COFs in the Photo-oxidation of Benzylamine



COF name (entry)	COF building blocks	band gap (eV)	yield, t_R	solvent	light source (power)
Por-sp2c-COF (i)	<i>p</i> -PdPor-CHO, PDAN	1.75	96% (0.8 h)	CH ₃ CN	white light (LED, 3 W)
Por-sp2c-COF (ii)	<i>p</i> -PdPor-CHO, PDAN	1.75	51% (0.25 h)	CH ₃ CN	$\lambda = 623$ nm (LED, 3W \times 4)
Por-sp2c-COF+TEMPO (iii)	<i>p</i> -PdPor-CHO, PDAN	1.75	94% (0.25 h)	CH ₃ CN	$\lambda = 623$ nm (LED, 3W \times 4)
TFPT-BMTH (iv)	TFPT, BMTH	2.74	99% (24 h)	H ₂ O	$\lambda = 454$ nm (LED, 30 W)

^a*p*-PdPor-CHO = [5,10,15,20-tetrakis(4-benzaldehyde)porphyrin], PDAN = 1,4-phenylenediacetonitrile, TFPT = 1,3,5-tris(4-formyl-phenyl)-triazine, BMTH = 2-methoxyethoxyterephthalohydrazide.

Scheme 13. (a) Por-sp2c-COF Application in Photo-oxidation of Primary and Secondary Amines with TEMPO as a Co-catalyst. (b) Mechanism for the Oxidation of Benzylamine under Visible-Light Irradiation Catalyzed by Por-sp2c-COF and TEMPO as a Co-catalyst^a

^aAdapted with permission from ref 47. Copyright 2020, Wiley–VCH GmbH.

for Por-sp2c-COF remarkably increases in the presence of TEMPO, which is beneficial for the oxidation of benzylamine.

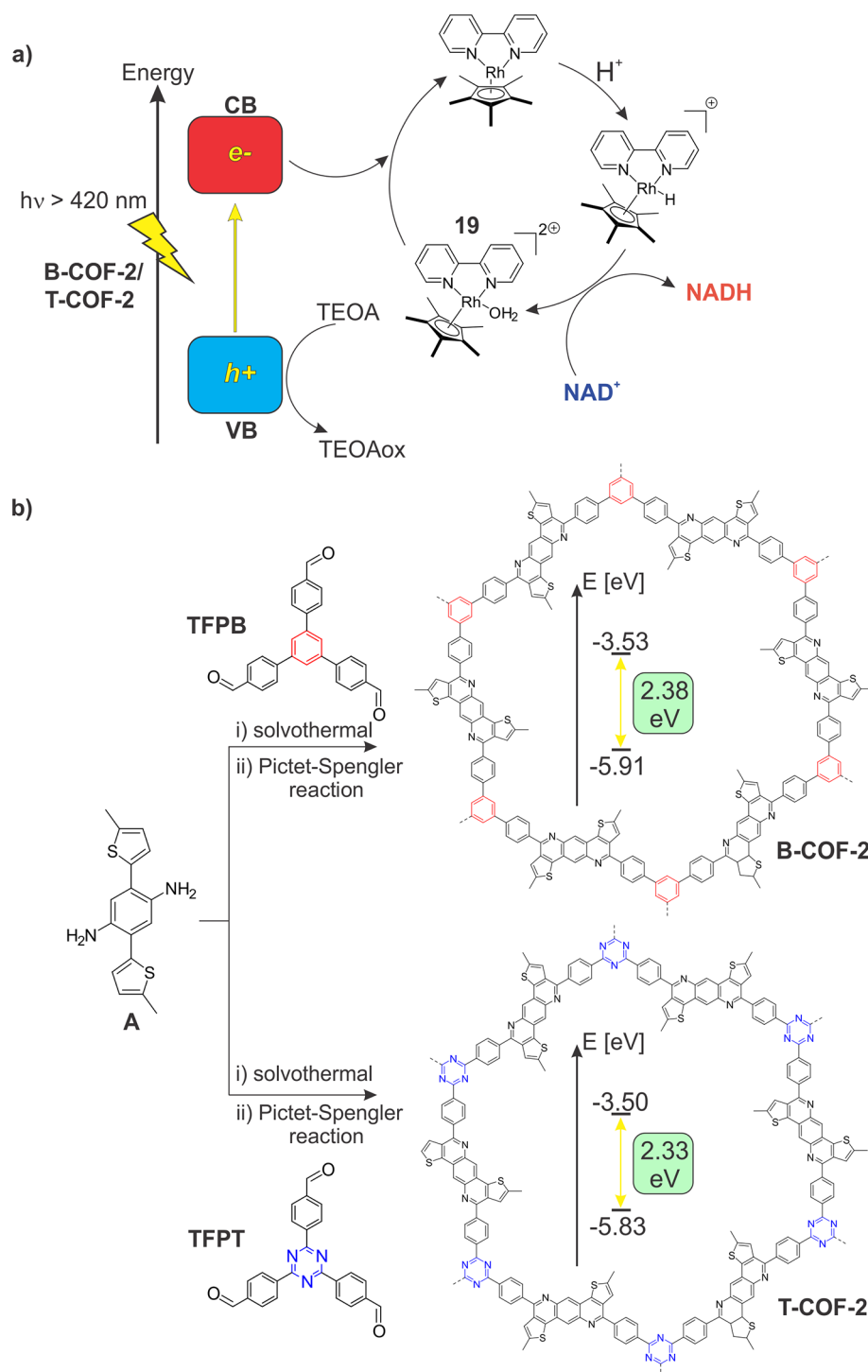
Importantly, benzylamine photo-oxidation by Por-sp2c-COF, in the presence of TEMPO, occurs with a doubled product yield, compared to the TEMPO-free setup (Table 5, entries (ii) and (iii)), thus indicating a synergy role played by the TEMPO cofactor, boosting the reaction efficiency. The stability of the Por-sp2c-COF photocatalyst was not addressed in subsequent reaction cycles.

A highly hydrophilic hydrazone-based COF, composed of 1,3,5-tris(4-formyl-phenyl)triazine (TFPT) and 2-methoxyethoxyterephthalohydrazide (BMTH) building blocks, TFPT-BMTH has been recently prepared and characterized by Yang and co-workers.⁴⁸ Incorporation of 2-methoxyethoxy groups into the channel walls of the framework makes the COF very

dispersible in water, which is a property exploited by the authors for the photocatalytic oxidation of benzylamine in aqueous solutions (Table 5, entry (iv)). Excellent product yield and selectivity have been achieved over a wide reaction scope with significant reusability of the catalytic system, the latter retaining fully its morphology and structure after five repeating cycles.

Reduction Reactions. Recent work by Zhao et al. showed how ultrastable and fully π -conjugated COFs can act as efficient photocatalysts for the nicotinamide adenine dinucleotide (NADH) regeneration.⁴⁹ B-COF-2 and T-COF-2 have been prepared in a two-step reaction: (i) condensation between building block A with 1,3,5-tri(4-formylphenyl)-benzene (TFPB) and 1,3,5-tris(4-formyl-phenyl)triazine (TFPT) building blocks under classical solvothermal con-

Scheme 14. (a) Mechanism for the Nicotinamide Adenine Dinucleotide (NADH) Regeneration under Visible-Light Irradiation Catalyzed by B/T-COF-2^a (b) Building Blocks and Reaction Conditions for the Synthesis of B-COF-2 and T-COF-2

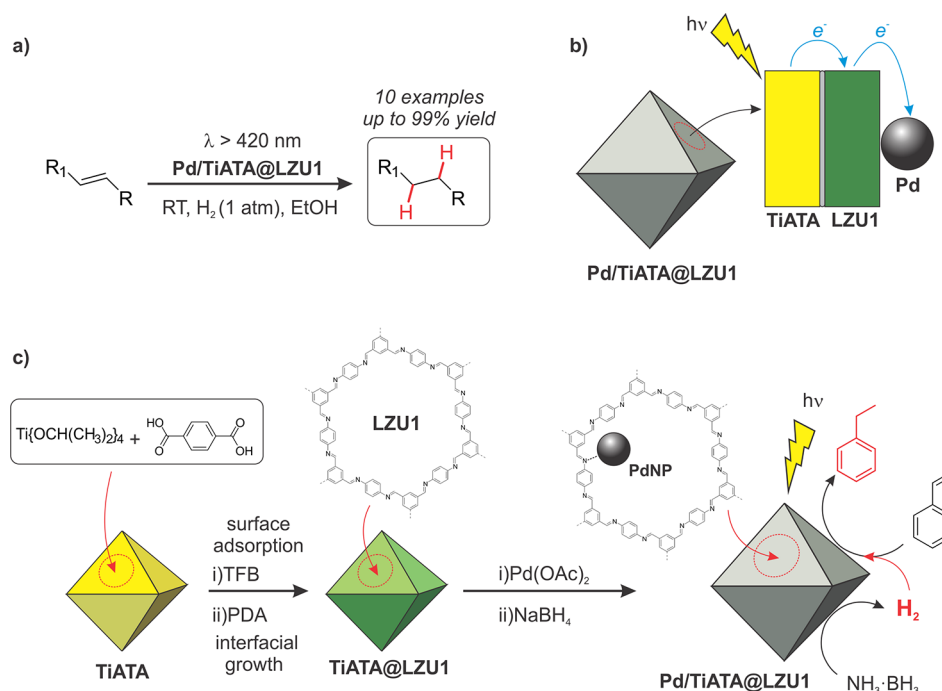


^aTEOA stands for triethanolamine employed as electron donor species. Adapted with permission from ref 49. Copyright 2020, American Chemical Society, Washington, DC.

ditions gives the imine-based crystalline **B-COF-1** and **T-COF-1** solids, respectively, and (ii) cyclization via the Pictet–Spengler reaction converts **B-COF-1** and **T-COF-1** to the thieno[3,2-*c*]pyridine-linked COF, **B-COF-2**, and **T-COF-2** (Scheme 14b). These post-modified COF showed exceptional thermal and chemical stability under harsh conditions. Moreover, both **B-COF-2** and **T-COF-2** have an extensive

absorption in the visible region (up to 650 nm) with a band gap of ~ 2.3 eV, while the CB and VB are respectively determined via cyclic voltammetry to be approximately -3.5 and -5.9 eV, respectively. Thus, these values indicated that both COFs possess the thermodynamic driving force to reduce the mediator $[\text{Cp}^*\text{Rh}(\text{bpy})-(\text{H}_2\text{O})]^{2+}$, **19**, the latter being responsible for transfer hydride to the NAD^+ species (Scheme

Scheme 15. (a) Pd/TiATA@LZU1 Application in Photocatalytic Hydrogenation of Olefins. (b) Proposed Electron Transfer Mechanism Occurring in Pd/Ti-ATA@LZU1, Where LZU1 Acts as a Charge-Transfer Mediator under Visible-Light Irradiation. (c) Schematic Illustration of the Preparation of Pd/Ti-ATA@LZU1 and Its Photocatalytic Application in the Hydrogenation of Olefins⁴⁴



⁴⁴Adapted with permission from ref 45. Copyright 2018, Wiley–VCH GmbH.

14a). Interestingly, while both imine-based COF, **B-COF-1** and **T-COF-1**, displayed negligible photoactivity, **T-COF-2** showed a dramatic increase of NADH regeneration (up to 74% within 10 min), compared to **B-COF-2**. These results have been ascribed by the authors to the extended conjugated structure of the thieno[3,2-*c*]pyridine-linked COFs coupled with the nitrogen-rich triazine core, which favors the binding of NAD⁺ by π – π stacking with the π -conjugated 2D surface of **T-COF-2**. Importantly, **T-COF-2** displayed remarkable photostability, since, after three reaction cycles, no obvious decrease in yield of NADH regeneration has been observed.

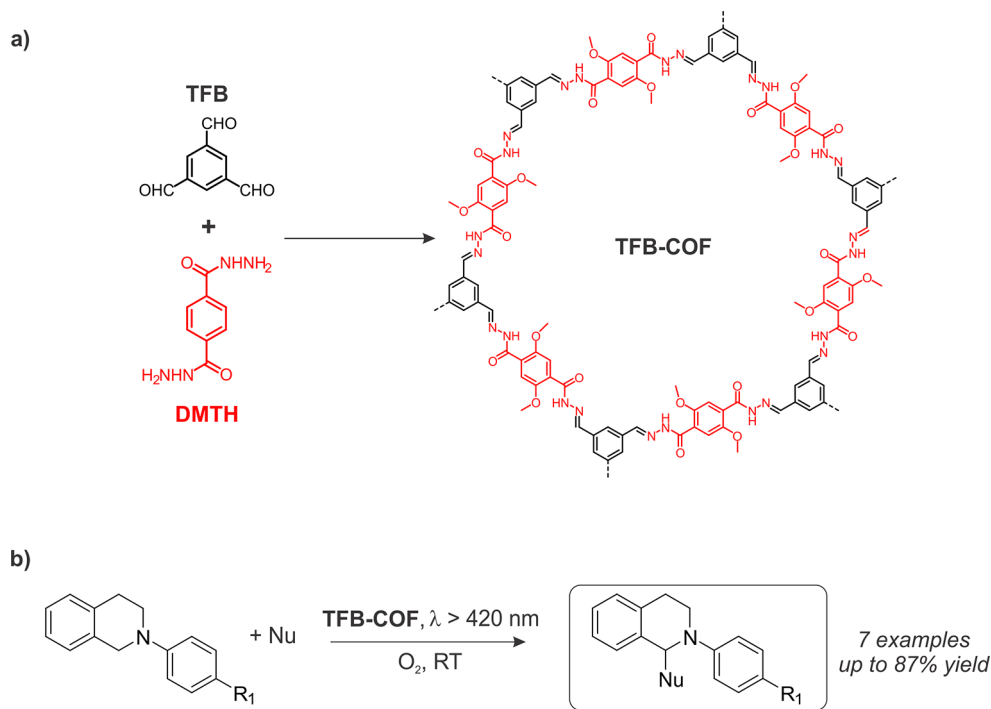
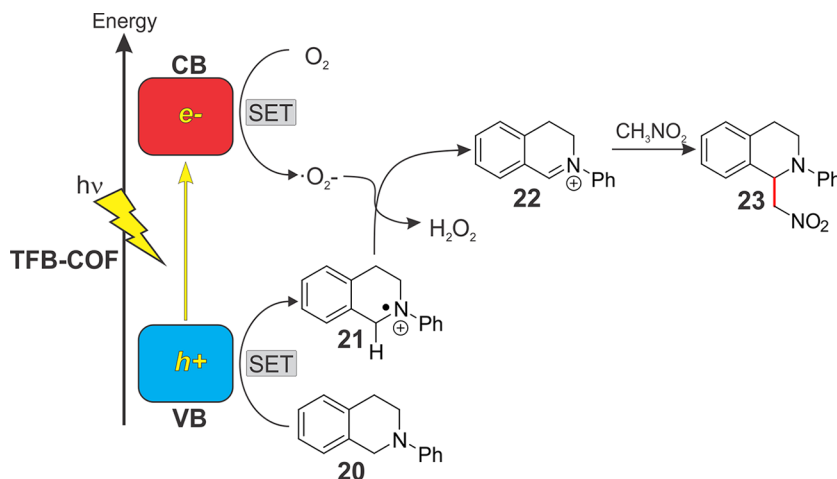
An elegant catalytic platform has been designed by Kim and co-workers for the photocatalytic hydrogenations of olefins employing a covalent organic framework acting as an ET mediator in a metal MOF@COF hybrid material.⁴⁵ In detail, the NH₂-MIL-125(Ti) denoted as **TiATA**, a known MOF photosensitizer, has been covered by vertically grown COF (**LZU1**) nanosheets by facile room-temperature synthesis exploiting the –NH₂ pendant functional groups of the starting MOF. Pd²⁺ has been then incorporated into the **TiATA@LZU1** material by leveraging the chelating ability of the imine bonds of the **LZU1** shell. A successive reduction of Pd²⁺ to Pd⁰ with NaBH₄ generated Pd nanoparticles with an average diameter of 2.2 nm, well-dispersed through the **TiATA@LZU1** material, as reflected by imaging analyses (Scheme 15c). The assembled material, **Pd/TiATA@LZU1**, shows an extended absorption up to 500 nm and displays a remarkable visible-light photocatalytic activity ($\lambda > 420$ nm) generating excellent yields (up to 99%) of hydrogenated products with high selectivity over a 10-example substrate scope (Scheme 15a). Pd species were confirmed to be the essential active sites to promote the hydrogenation reaction, while visible light is needed to

promote the catalytic activity, because a substantial decrease in yield is observed under dark conditions. Notably, the photocatalytic activity decreases in the absence of the **LZU1** highlighting the positive synergistic effects among the **TiATA** core, the **LZU1** COF shell, and the doped Pd metal. Indeed, emission quenching experiments suggest that **LZU1** acts as an electronic mediator promoting the electron transfer from the excited **TiATA** to Pd species, thus the **Pd/TiATA@LZU1** can be viewed as a “donor–mediator–acceptor” system (Scheme 15b).

The **Pd/Ti-ATA@LZU1** catalytic system has also been successfully tested in tandem dehydrogenation and hydrogenation photoreactions employing a novel designed dual-chamber microreactor featuring two circular reaction compartments separated by a gas-permeable PDMS membrane, each of them loaded with **Pd/TiATA@LZU1**. The reagents, NH₃·BH₃ complex and desired olefin, were separately injected through four inlets into the dual chamber reactor under light irradiation ($\lambda > 420$ nm) and in continuous flow configuration. The hydrogen generated in situ by the photocatalytic dissociation of ammonia-borane complex could smoothly pass through the PDMS membrane and thus convert the olefin to the corresponding alkane. As highlighted by the authors, such a photocatalytic system can potentially be extended to challenging liquid–gas and cascade reactions.

Carbon–Carbon Bond Formation. Forging new carbon–carbon bond connectivity is one fundamental transformation to increase complexity in organic synthesis.⁶³ Photocatalysis is at the forefront of an intense research effort to develop sustainable synthetic methods including cross-dehydrogenative coupling (CDC), a versatile methodology for the selective construction of C–C bonds from two different

Scheme 16. (a) Synthesis of TFB-COF Starting from the Building Blocks TFB and DMTH. (b) TFB-COF Application in CDC Reaction

Scheme 17. Mechanism for the CDC Reaction under Visible-Light Irradiation Catalyzed by TFB-COF⁴²

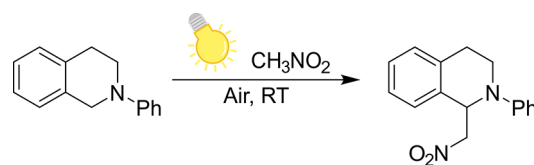
⁴²Adapted with permission from ref 50. Copyright 2016, Wiley-VCH GmbH.

C–H bonds without the need of substrate preactivation.^{13,64,65} Below are some remarkable examples where COFs have been employed as photocatalysts for C–C bond formation.

Cross-dehydrogenative coupling (CDC) reactions between tetrahydroisoquinoline (THIQ) and various nucleophiles have been successfully tested using a hydrazone-based COF, TFB-COF, as visible light photocatalyst material by Wu et al. in 2017.⁵⁰ TFB-COF has been synthesized by acid-catalyzed reversible condensation between 1,3,5-triformylbenzene (TFB) and 2,5-dimethoxyterephthalohydrazide (DMTH) building blocks (Scheme 16a). IR, CP/MAS ¹³C NMR, and BET analyses confirmed the crystalline and porous structure of TFB-COF, while a diffuse reflectance UV–vis spectrum displayed an absorption edge at ca. 450 nm, corresponding to an optical band gap of 2.88 eV.

The reaction mechanism can be summarized in the following steps: (i) generation of THIQ radical cation **21** from **20** by the hole generated at the TFB-COF-VB via a single electron transfer process (SET), (ii) reduction of O₂ to superoxide radical anion by the electrons promoted at the TFB-COF-CB, (iii) proton abstraction from the α-amino C–H bond of THIQ⁺ **21** by •O₂[−] species to form the THIQ iminium ion **22**, and (iv) nucleophilic addition (e.g., CH₃NO₂) to the THIQ iminium ion **22** to yield the final product **23** (Scheme 17). Good product yields with high selectivity have been obtained over a wide substrate scope (Scheme 16b, Table 6, entry (i)), and, importantly, TFB-COF is provided to be a robust photocatalyst, since its catalytic activity has been fully retained after three reaction cycles.

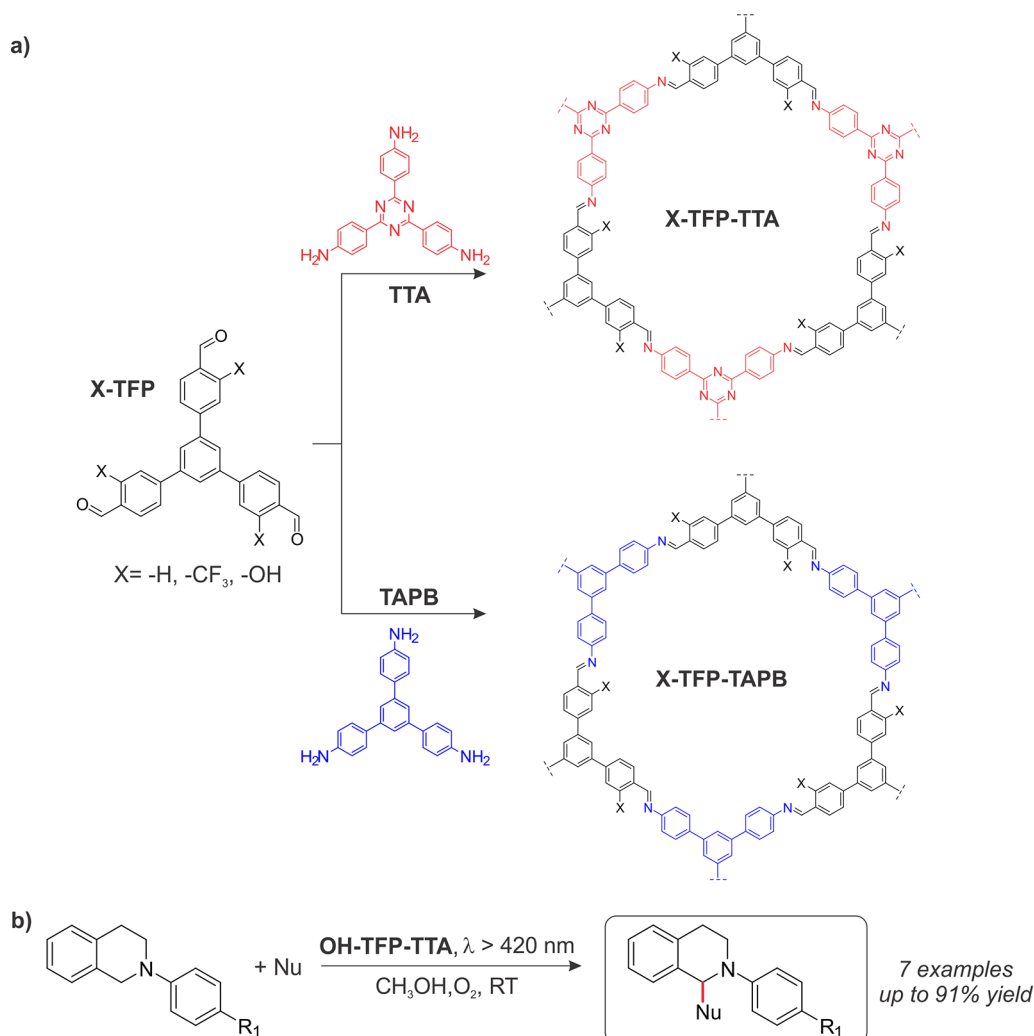
Table 6. Comparison of the Catalytic Performance of COFs for the Photo-induced CDC Reaction between Tetrahydroisoquinoline (THIQ) and Nitromethane^a



COF name (entry)	building blocks	band gap (eV)	yield, t_R	light source (power)
TFB-COF (i)	DMTH, TFB	2.88	87% (36 h)	energy-saving lamp (45 W)
COF-JLUS (ii)	TTA, DMTP	/	99% (6 h)	$\lambda = 460$ nm (LED, 30 W)
OH-TFP-TTA (iii)	OH-TFP, TTA	2.60	93% ^b (6 h)	$\lambda = 460$ – 470 nm (LED, 30 W)
COF-1, COP-1 (iv)	NBC, ETTA	2.24	85%, ^c 76% (40 h)	$\lambda = 440$ nm (LED)
COF-2, COP-2 (v)	TAPB, ETBC	2.14	83%, ^c 70% (40 h)	$\lambda = 440$ nm (LED)

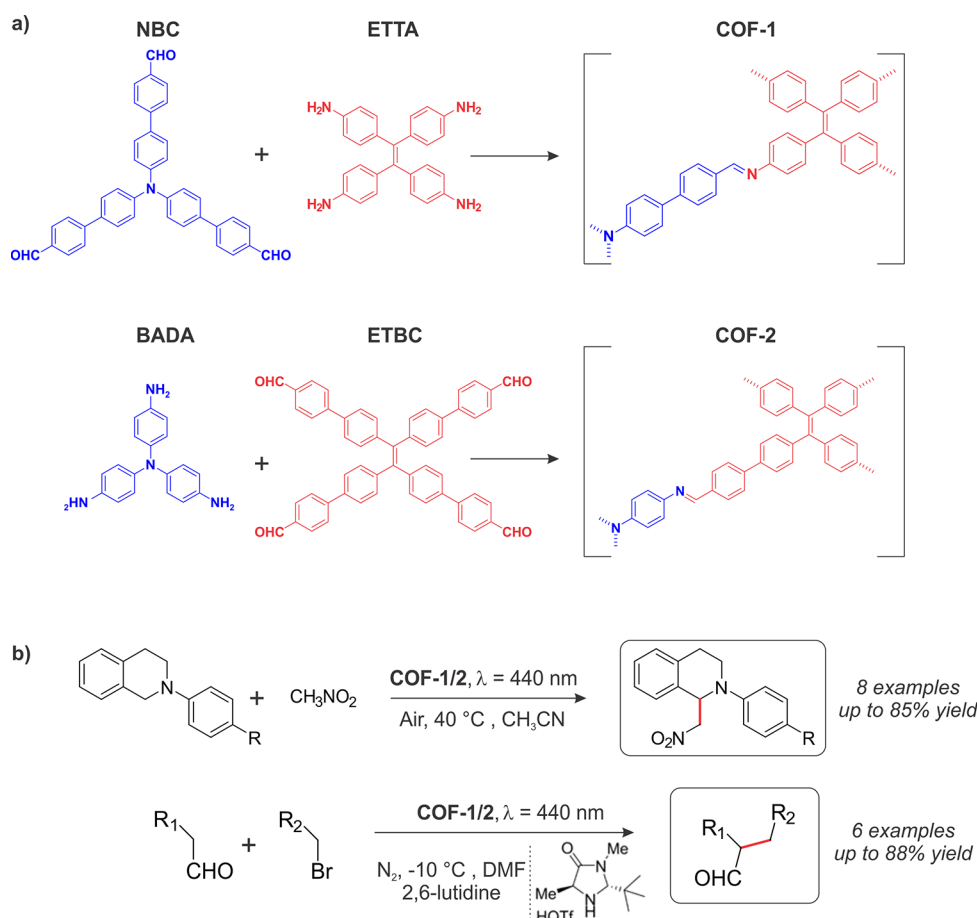
^aAbbreviations used: DMTH = 2,5-dimethoxyterephthalohydrazide, TFB = 1,3,5-triformylbenzene, DMTP = 2,5-dimethoxyterephthalaldehyde, OH-TFP = 1,3,5-tris(4-formyl-3-hydroxyphenyl)-benzene, TTA = 4,4',4''-(1,3,5-triazine-2,4,6-triyl)trianiline, NBC = 4',4''',4''''-nitrotris([1,1'-biphenyl] 4-carbaldehyde), ETTA = tetrakis(4-aminophenyl)ethylene, TAPB = tris(4-aminophenyl)amine, ETBC = 4',4''',4''''-(1,2-ethenediylidene)tetrakis[1,1'-biphenyl]-4-carboxaldehyde. ^bN-(*p*-Tolyl)-1,2,3,4-tetrahydroisoquinoline as the substrate. ^cN-(*p*-Tolyl)-1,2,3,4-tetrahydroisoquinoline as the substrate, under air and 40 °C.

Scheme 18. (a) Synthesis of 2D-COFs by the Condensation Reaction between TFP *ortho*-Substituted on the Peripheral Ring and TTA/TAPB Building Blocks. (b) OH-TFP-TTA Application in CDC Reaction



The CDC reaction was also explored by Liu et al. in the same year, employing a new imine-based COF as a photocatalyst, COF-JLUS, synthesized under solvothermal conditions by condensation of 4,4',4''-(1,3,5-triazine-2,4,6-

triy)trianiline (TTA) and 2,5-dimethoxyterephthalaldehyde (DMTP) (Table 6, entry (ii)).⁵⁴ The methoxy substituents as electron-rich groups stabilize the Schiff-base centers imparting stability to the COF framework. Indeed, no

Scheme 19. (a) Building Blocks for the Synthesis of COF-1 and COF-2. (b) COF-1/COF-2 Application in CDC Reaction and Asymmetric α -Alkylation of Aldehydes

structural changes have been observed when COF-JLU5 has been dispersed for several days in either acidic (HCl, 12 M) and basic environment (NaOH, 14 M). Good to excellent yields with high selectivity have been observed for a wide substrate scope in CDC reactions, including the formation of α -amino dialkyl phosphonates products. Notably, COF-JLU5 displayed remarkable recyclability; indeed, the reused material, isolated by simply centrifugation, fully retained its catalytic activity as well as its structure, even after 10 subsequent cycles.

A series of 2D-COFs, synthesized by the condensation reaction between 1,3,5-tris(4-formylphenyl)benzene, *ortho*-substituted on the peripheral ring with $-\text{OH}$ and $-\text{CF}_3$ groups (X-TFB), with 4,4',4''-(1,3,5-triazine-2,4,6-triyl)-trianiline (TTA) and tris(4-aminophenyl)amine (TAPB) building blocks (Scheme 18a), have been recently tested in CDC (Scheme 18b, Table 6, entry (iii)) and dehalogenation reactions by Tang, Li, and co-workers.⁵⁵ Photophysical and electrochemical characterizations including optical band gap determination, photocurrent response, and EIS (electrochemical impedance spectroscopy) concluded that the COF composed by triazine framework (TTA) and TFB bearing $-\text{OH}$ group (OH-TFP-TTA) has the best visible-light absorption ability (broad absorption up to ca. 570 nm, band gap of 2.6 eV), as well as an optimal charge-transfer efficiency. Indeed, the highest product yields in both photochemical reactions tested have been observed for OH-TFP-TTA, which also showed the ability to retain catalytic activity and crystallinity after several reaction runs. Importantly, the

amorphous counterpart of OH-TFP-TTA displayed a much lower product yield (90% vs 18%), indicating that the ordered 2D porous structure plays a key role in improving the photocatalytic activity, likely due to the reticular porous structure.

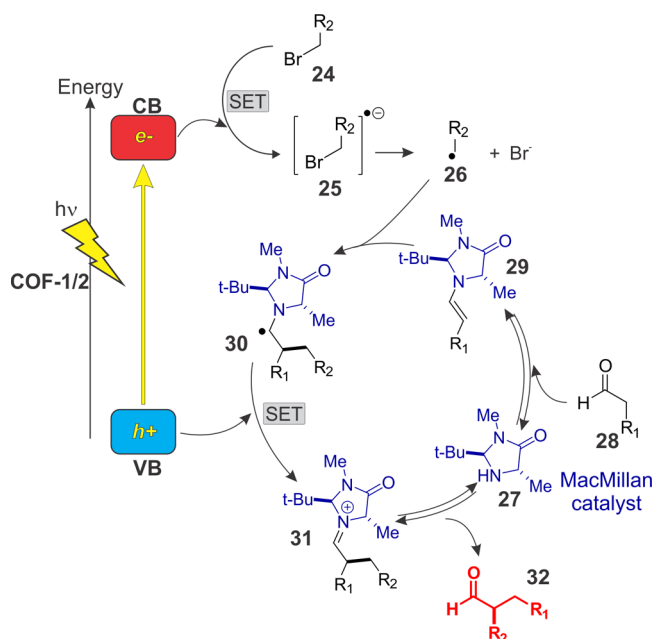
In very recent work, Cui et al. explored the CDC reaction (see Scheme 19b, and Table 6, entries (iv) and (v)) using two novel 3D-COF as a photocatalyst, COF-1 and COF-2, prepared starting from triphenylamine and tetraphenylethene derivatives as the functional building blocks (Scheme 19a).⁵⁶ Unlike most of the 3D-COFs, the corresponding building blocks of COF-1/COF-2 do not possess tetrahedral geometry but, because of their propeller-like structures under solvothermal conditions, yielded a 3D porous frameworks with a rare 2-fold-interpenetrated topology (ffc).

Notably, both COF-1 and COF-2 have absorption edges at ~ 554 and 579 nm , corresponding to band-gap values of 2.24 and 2.14 eV, respectively; thus, both COFs serve as ideal visible-light photocatalysts. Indeed, excellent yields, particularly with the THIQ substrate bearing electron donor groups, have been reported using both COF-1 and COF-2 under blue-light irradiation ($\lambda = 440 \text{ nm}$). Most importantly, for the first time, COF materials have been combined with a chiral imidazolidinone organocatalyst for enantioselective transformations, and specifically used for the asymmetric α -alkylation of aldehydes (Scheme 19b). The concept of merging photoredox with organo-catalysis was first explored by the group of MacMillan.⁶⁶ From this seminal work, diverse combinations

of dual organocatalytic/photoredox systems have been explored.⁶⁷ For instance, metal-based sensitizers ($\text{Ru}(\text{bpy})_3\text{Cl}_2$, $[\text{Fe}(\text{bpy})_3]^{2+}$), semiconductor bismuth-oxides (Bi_2O_3) and organic dyes (eosin Y) were found to be competent photocatalysts for the enantioselective α -alkylation of aldehydes.^{68–70}

The plausible mechanism proposed for the asymmetric α -alkylation of aldehydes catalyzed by the COF1 and COF2 with an imidazolidinone organocatalyst is depicted in Scheme 20.

Scheme 20. Plausible Mechanism for the Asymmetric α -Alkylation of Aldehydes under Visible-Light Irradiation Catalyzed by COF-1/COF-2



Upon excitation, the electron promoted on the COF-CB is transferred to the electron-acceptor bromo-compound 24 via single electron transfer (SET) to generate the corresponding radical anion 25, which, via rapid fragmentation of the C–Br bond, releases the electrophilic radical 26. Concurrently, the imidazolidinone catalyst 27 activates the aldehyde 28 via enamine (29) formation. The electrophilic radical 26 engages in a stereodetermining C–C bond-forming event with the enamine 29 yielding the α -amino radical 30, which is prone to oxidation by the COF-VB. The photoredox cycle is thus closed. The hydrolysis of the iminium ion 31 provides the desired alkylated aldehyde 32, while the imidazolidinone can restart another catalytic cycle.

Table 7 collects representative dual photo-organocatalytic systems for the enantioselective α -alkylation of aldehydes, using the chiral imidazolidinone 27 as organocatalyst. Remarkably, both COF-1 and COF-2 gave comparable results, in terms of product yield and ee (enantiomeric excess), with respect to molecular photocatalysts. Although the COF-based systems require longer reaction time and low-temperature conditions, this work paves the way for the development of COF-based photocatalysts combined with small molecule activators, thus opening a broad application scenario. Interestingly, the authors performed host–guest experiments (e.g., substrate uptake, fluorescence quenching titration) which seem to corroborate that the photochemical reaction is

occurring within the COF porous structure, although size-selective experiments with different sterically aromatic aldehydes failed to confirm this hypothesis.

In the reactions tested, CDC and α -alkylation of aldehydes, both COF-1 and COF-2 lost their crystallinity, which could be easily recovered via solvent-assisted linker exchange strategy, i.e., by exposing the amorphous COF to a solution excess of starting building blocks under solvothermal conditions. Interestingly, in the aldehyde α -alkylation reaction, the amorphous materials (COP-1 and COP-2) behave similarly to the corresponding crystalline materials, in terms of ee values but with $\sim 10\%$ lower product yields, suggesting that the crystallinity may facilitate the substrate adsorption/activation and enhance electron transfer from the COF-CB to the α -bromocarbonyl substrate.

Recently, Liu et al. explored the photocatalytic activity of COF-JLU22, obtained from the condensation between 1,3,6,8-tetrakis(4-amino-phenyl)pyrene (PyTTA) and 4,4-(benzothiazole-4,7-diyl)dibenzaldehyde (BTDA), toward the α -alkylation of aldehydes, using tetrahydropyrrole as an achiral organocatalyst.⁵⁷ In the same work, the authors tested COF-JLU22 also in photoreductive dehalogenation reactions, specifically of phenacyl bromide and its derivatives. Apart from good product yields in both reactions tested, the COF photocatalyst also showed high recyclability. Indeed, no significant loss of catalytic activity has been observed after five reaction cycles together with structural conservation of the recycled material. Importantly, the filtrated reaction mixture solution did not display further photocatalytic activity, indicating that the process is purely heterogeneous and confirming the photostability of COF-JLU22 under the reaction conditions.

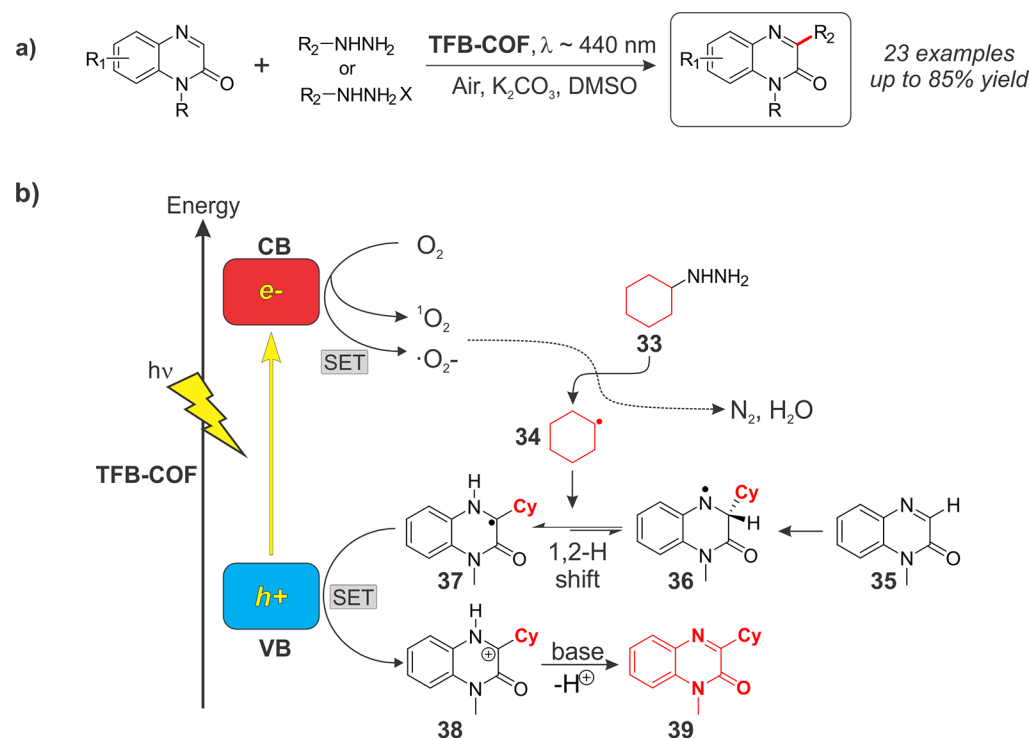
Employing TFB-COF (see Scheme 16a for structure) as a heterogeneous photocatalyst, Yang and co-workers investigated the C3 arylation and alkylation of quinoxalin-2(1H)-ones, important molecules widely present in pharmaceutical drugs as core structures (Scheme 21a).⁵¹ The proposed reaction mechanism by the authors is depicted in Scheme 21b. Visible-light irradiation triggers at the TFB-COF-CB the reduction and/or energy transfer of O_2 into superoxide radical anion and/or singlet oxygen, which, in turn, reduce the hydrazine 33 to the corresponding carbon-centered radical 34 releasing H_2O and N_2 . The addition of 34 to the quinoxalin-2(1H)-one 35 yields the α -amino radical 36, followed by a 1,2-H shift to give 37. The latter radical species 37 is then oxidized, by the holes accumulated at the TFB-COF VB, to the cation 38, which, in turn, is deprotonated to give the desired product 39.

Importantly, TFB-COF showed excellent photostability; even after six reaction cycles, the loss of catalytic activity is negligible, which is instrumental for gram-scale synthetic application, as successfully reported.

Alkylation of quinoxalin-2(1H)-ones and related heterocycles (e.g., isoquinolines, quinolines) via photocatalytic decarboxylative generation of carbon-centered radicals have also been explored recently by Yang and co-workers, where they tested four imine-linked 2D-COFs and one olefin-linked COF (2D-COF-2) as heterogeneous photocatalysts.⁵⁸ The proposed reaction mechanism occurs similarly to that described in Scheme 21b, whereby the generation of carbon-centered radicals occurs upon reduction of *N*-hydroxyphthalimide (NHPI) esters ($E = -1.20$ V vs SCE) by the 2D-COF-2-CB ($E = -1.40$ V vs SCE) which delivers the desired alkyl

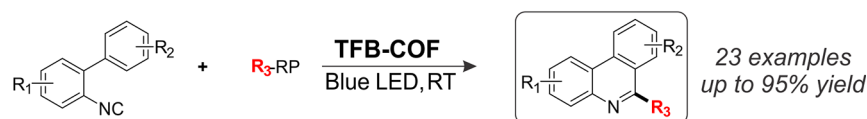
Table 7. Comparison of Dual Catalytic Systems for the Enantioselective α -Alkylation of Aldehydes

Photocatalyst (Reaction time)	Selected scope		
Ru(bpy) ₃ Cl ₂ (5-7 hrs)	92% yield, 90% ee	93% yield, 90% ee	83% yield, 95% ee
Bi ₂ O ₃ (2 hrs)	86% yield, 93% ee	85% yield, 91% ee	81% yield, 98% ee
Fe(bpy) ₃ Br ₂ (16 hrs)	83% yield, 92% ee	82% yield, 92% ee	75% yield, 97% ee
Eosin Y (18 hrs)	76% yield, 86% ee	82% yield, 95% ee	not reported
COF-1 (40 hrs, -10 °C)	83% yield, 94% ee	88% yield, 90% ee	78% yield, 91% ee
COF-2 (40 hrs, -10 °C)	80% yield, 94% ee	85% yield, 91% ee	76% yield, 90% ee

Scheme 21. (a) TFB-COF Application in the Alkylation of Quinoxalin-2(1H)-one. (b) Mechanism for the Alkylation of Quinoxalin-2(1H)-one under Visible Light Irradiation Catalyzed by TFB-COF^a^aAdapted with permission from ref 51. Copyright 2019, Wiley-VCH GmbH.

Scheme 22. (i) Radical Addition–Cyclization of 2-Aryl Phenyl Isocyanides and (ii) Oxidative N–S Bond Formation Catalyzed by TFB-COF under Visible-Light Irradiation

i) Radical addition-cyclization of 2-aryl phenyl isocyanides



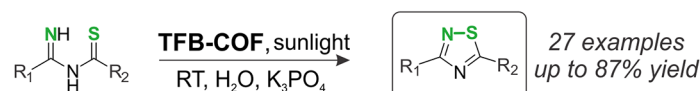
R_3 = Ar, Alkyl (Reaction conditions: Air, DMSO, K_2CO_3)

R_3 = CF_3 , (Reaction conditions: N_2 , EtOAc, Na_2CO_3 , $K_2S_2O_8$)

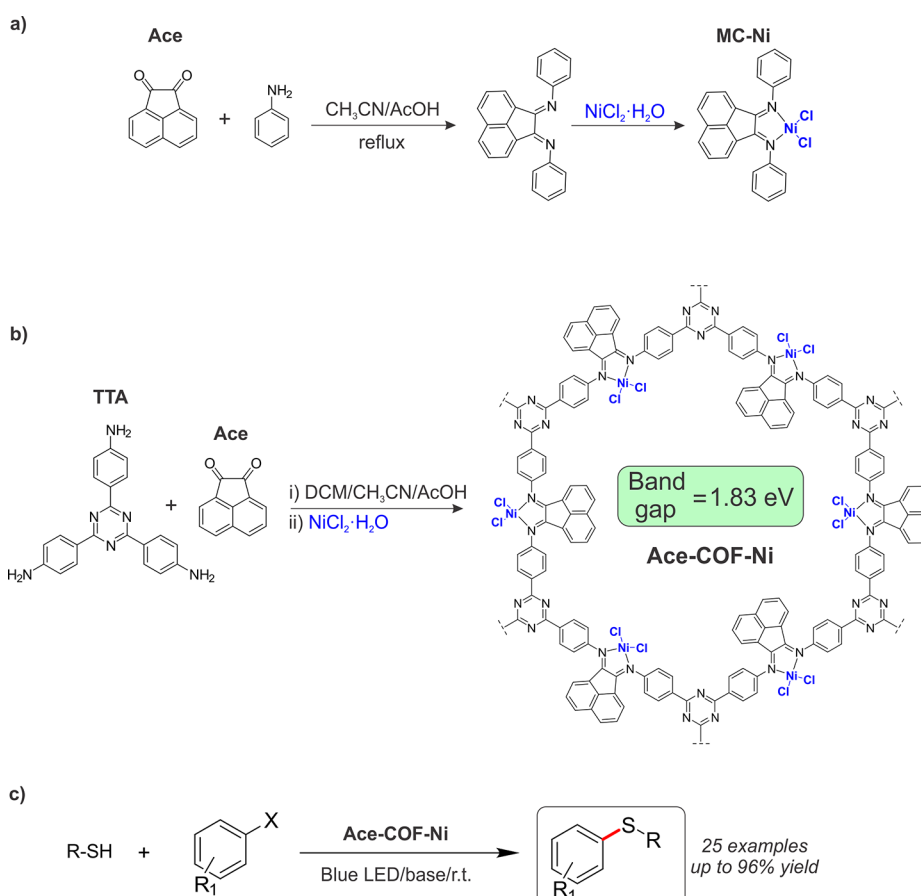
R_3 = (O)PAr₂ (Reaction conditions: N_2 , EtOAc, CsF, $K_2S_2O_8$)

R_3 = ArS (Reaction conditions: N_2 , EtOAc, Di-tert-butyl peroxide)

ii) Oxidative construction of N–S bond



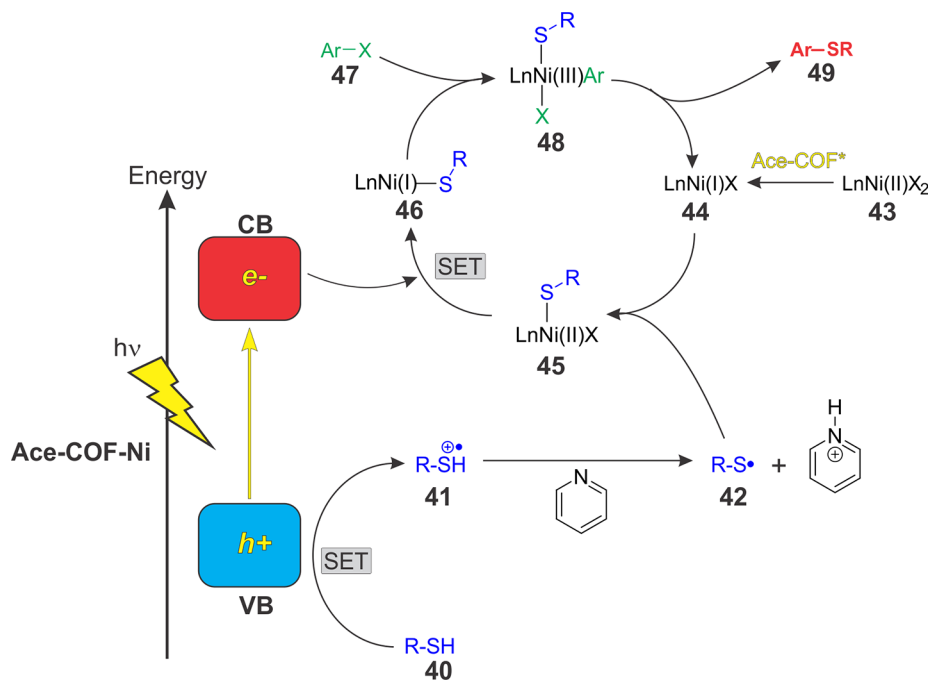
Scheme 23. (a) Synthesis of the Model Compound MC-Ni. (b) Building Blocks and Reaction Conditions for the Synthesis of Ace-COF-Ni. (c) Ace-COF-Ni Application in the S–C Cross-Coupling Reaction



radical and CO_2 as a side product. The **2D-COF-2** displayed the highest catalytic performance among the COFs investigated while maintaining the porous and ordered structure for six reaction cycles. Importantly, the authors extended the substrate scope to derivatives from natural products and pharmaceutical drugs, including a gram-scale reaction of isoquinoline derived from lithocholic acid, showing the potential of COFs as industrial photocatalysts.

Other Relevant Reactions. The hydrazone-based COF, TFB-COF, has also been employed by Yang and co-workers as

visible-light photocatalyst for cyclization reactions, namely, (i) radical addition-cyclization of 2-aryl phenyl isocyanides for the synthesis of 6-substituted phenanthridines,⁵² and (ii) the oxidative construction of N–S bond for the preparation of 1,2,4-thiadiazoles (Scheme 22).⁵³ From good to excellent product yields have been obtained in both reactions tested for a wide substrate scope making the TFB-COF as efficient as the molecular photocatalyst alternatives. Importantly, the COF material could be recycled and reused for several consecutive reaction cycles without appreciable loss of catalytic activity, as

Scheme 24. Mechanism for the S–C Cross-Coupling Reaction under Visible-Light Irradiation Catalyzed by Ace-COF-Ni^a

^aAdapted with permission from ref 59. Copyright 2021, Wiley–VCH GmbH.

reflected by the conservation of the corresponding porous and ordered framework. Scaled-up experiments in a continuous flow have also been performed, with both reactions giving the desired product in high yield, which can pave the way for large-scale production.

Apart from the work of Aleman et al., where metal catalyst (Pt) has been incorporated in a photoactive COF framework (see Scheme 10a) by truncation strategy, the rest of the examples dealing with COF as a catalytic system for organic transformations focus on employing COF in the absence of metal cofactors. In a very recent paper, Voort and co-workers explored the application of COF by combining the photoredox ability of the organic framework with a transition-metal catalyst (metallo-photoredox catalysis) to drive sulfur–carbon cross-coupling reaction employing visible-light irradiation.⁵⁹ In detail, a new photosensitive triazine-based COF has been prepared by condensation reaction between 4,4',4''-(1,3,5-triazine-2,4,6-triyl)trianiline (TTA) and acenaphthenequinone (Ace) to give the corresponding porous and crystalline COF (Ace-COF). The Ace-COF features topologically ordered D–A heterojunctions, known to photogenerated long-lived charge carriers essential for enhanced photocatalytic activity. By exploiting the chelating property of 1,2-bis(phenyl)-acenaphthene moiety, Ni ions have been introduced into the COF through a simply wet impregnation process consisting of soaking the Ace-COF with NiCl₂·H₂O methanol solution to give the corresponding Ace-COF-Ni material (Scheme 23b).

Extensive characterization of the resulting material confirmed the presence of Ni into the crystalline and porous structure of Ace-COF-Ni, revealing an enhanced absorption in the visible light range (up to 700 nm) corresponding to a band gap of 1.83 eV. Therefore, the authors evaluated the potential of Ace-COF-Ni as a metallo-photoredox catalyst, in a model reaction, that is the cross-coupling between iodobenzene and thiophenol in the presence of pyridine as a base under blue-light irradiation (LED, 420 nm < λ < 430 nm). Excellent

product yield has been obtained after 24 h of continuous irradiation at room temperature, while control tests show how the catalytic activity benefits from the proximity of the photosensitizing COF scaffold with Ni active sites. Indeed, under the same reaction conditions, the product yield decreased from 95% to 26% when the benchmark reaction has been tested employing a physical mixture of pristine Ace-COF and the model compound MC-Ni (Scheme 23a) acting respectively as photoredox material and metal catalytic site. A detailed mechanistic investigation including time-resolved emission spectroscopy, steady-state emission quenching experiments, EPR spectroscopy, and cyclic voltammetry point to the reaction mechanism depicted in Scheme 24, where the Ni(I) are the active species in the catalytic cycle. Upon visible-light irradiation, the holes generated in the Ace-COF-Ni-VB are quenched via SET process from the thiol 40 to generate the corresponding radical cation 41, which, in turn, is converted to the thiol radical 42 after being deprotonated by pyridine. The thiol radical 42 then oxidatively adds to Ni(I)-halide 44, generated in turn by the reduction of the starting Ni(II)-halide 43 from the photoexcited Ace-COF-Ni, to yield the Ni(II)-sulfide complex 45. The latter species is then reduced by the Ace-COF-Ni-CB via SET to form the Ni(I)-sulfide species 46. Oxidative addition of aryl halide 47 to the Ni(I)-sulfide complex 46 forms the Ni(III) complex 48, which delivers the S–C cross-coupled product 49 upon reductive elimination step. Therefore, the proximity between the photoactive framework and the Ni catalytic sites improves the overall catalytic efficiency, since it facilitates the electron transfer as well as the oxidative addition of thiol radical 42 to the Ni complexes 45 and 44, respectively. Importantly, the Ace-COF-Ni material displayed wide applicability and recyclability as witnessed by the large substrate scope (Scheme 23c) and a negligible loss of catalytic performance after five consecutive reaction cycles.

Banerjee and co-workers recently explored the visible-light photoassisted *E* to *Z* isomerization of olefins via energy transfer process employing a photoactive COF, **TpTt**, prepared by the condensation of melamine with 1,3,5-triformylphloroglucinol (Tp) building block.⁷¹ Importantly, the triazine core framework of **TpTt** should preferentially form complexes with *E* olefin by π - π stacking interaction, thus selectively transfers the energy to this isomer.⁶⁰ As a result, the photoequilibrium is shifted from the thermodynamically more stable (*E*) to the energetically less stable form of olefin (*Z*).

The ordered and porous structure of **TpTt** has been confirmed by PXRD, BET, and FT-IR among others, while solid-state UV-vis diffuse reflectance spectroscopy displayed an extended visible absorption up to \sim 530 nm with an optical band gap of 2.74 eV, making **TpTt** an ideal photocatalyst for the visible-light-assisted isomerization of olefins. Indeed, excellent conversions have been observed for a wide substrate scope, e.g. *trans*-stilbene reached a maximum conversion of 90% to the corresponding *cis* isomer under 18 h of irradiation with blue-light LED. **TpTt** also showed remarkable recyclability, after four reaction cycles no loss of photocatalytic activity has been observed coupled with the full conservation of the initial structure, as witnessed by FT-IR, PXRD, and TEM analysis. In addition, the authors explored the crystallinity effect of **TpTt** material as a function of photocatalytic activity. The conversion of *trans* to *cis*-stilbene decreased from 90% to 8% when switching from the crystalline **TpTt** to the amorphous counterpart, which may indicate that the reaction is occurring within the COF pores or at the crystallite surface since the length of the substrate (\sim 1.1 nm) is not compatible with the determined **TpTt** pore size distribution ($\eta \approx$ 1.3 nm).

CONCLUSIONS AND OUTLOOK

Covalent organic frameworks represent an emerging class of porous, lightweight, and crystalline materials, whose applications are constantly rising in many different fields spanning from molecular chemistry to photophysics and materials engineering, thus reflecting their high potential and emergent properties. Recently, COFs have been employed as novel photocatalysts to induce organic transformations under mild and sustainable reaction conditions. COF-based photocatalysis is mostly centered on the materials science aspects, that is, on the design, characterization, and understanding of the COF structural features, rather than on the emerging reactivity patterns originating from the ordered framework of their functional components. In particular, the advantage of confinement effects, intrinsic to the porous and long-range ordered structure of COF materials, is largely underrated. Indeed, few works address the photoreactivity and product selectivity as a function of the COF pore size, albeit preliminary results indicate that the substrate dimension is one parameter affecting the photocatalysis kinetics and selectivity, in relation to the COF pore diameter.^{39,42,71} Noteworthy, the impact of particle size of photoresponsive COF materials is yet to be explored, although it is well-established to be one key parameter influencing the photocatalytic performance of inorganic semiconductors, e.g., TiO₂.⁷² Therefore, systematic and mechanistic studies are needed to trace structure-activity relationships with predictive potential, for COF optimization, in terms of performance, selectivity, and substrate scope.

Importantly, COF scaffolds are amenable to post-functionalization strategies, with negligible loss of the pristine crystallinity, making them ideal for the colocalization of light-harvesting/conversion domains with catalytic cofactors, wherein the former function originates from the π -conjugated COF skeleton, while catalytic sites can be anchored on the pore surfaces. The recent work by Voort and co-workers explored such proximity and confinement effects in detail so that excellent photocatalytic performance has been observed for the sulfur-carbon cross-coupling reactions.⁵⁹ Moreover, as demonstrated in recent case studies highlighted herein,^{37,38} COFs possess high adaptability to combine with complementary materials (e.g., inorganic semiconductors and MOF), which generate photoactive interfaces capable to significantly retard electron-hole recombination, a crucial feature for efficient photoinduced electron transfer processes. In this vein, COFs have also been successfully coupled with carbon nanostructures, through template synthesis, e.g., using graphene or carbon nanotubes, providing composite materials with exceptional mechanical and electrochemical properties, and notable interest for photocatalytic transformations.⁷³⁻⁷⁶

It turns out that COF materials have all the advantages of heterogeneous catalysts, including easy recovery and reuse of the solid material, a property widely valued for large-scale production. Indeed, recent progress in the COF chemical synthesis is delivering innovative structures featuring ultra-stability, which is key to facilitating their transferability to industrial applications. One major bottleneck for the cost-effective, sustainable production of COFs and of related materials, e.g., MOF, has been ascribed to the solvothermal synthetic protocol. In this regard, a 50% cut of production costs is expected by switching from the classical solvothermal approach, employing large quantities of expensive organic solvents, to a liquid-assisted grinding method (LAG) or aqueous synthesis.⁷⁷ Furthermore, process intensification under continuous synthesis operation,⁷⁸ might provide a convenient approach to improve the cost efficiency and the environmental sustainability of COFs manufacture.

Thus, COF materials have all the prerequisites to become a reference platform for photocatalytic transformations, especially applied to advanced synthetic methods. Prominent examples include not only classical transformations of functional groups, but also the challenging construction of C-C bonds in asymmetric environment, as in the case of the enantioselective α -alkylation of aldehydes,⁵⁶ and the cross-dehydrogenative coupling (CDC) reactions,⁵⁰ while the reported sulfur-carbon cross-coupling reaction through a COF dual catalyst strategy is remarkable.⁵⁹ These examples open several possibilities to solve modern organic synthesis problems. The maturity of this field will be key for the development of COF-based photocatalysts with application in synthetic chemistry.

COFs may bridge the gap between molecular and heterogeneous catalysis, thus opening new avenues to trigger multifunctional activation strategies. However, producing COFs that are simultaneously crystalline, stable, and functional (the COF trilemma)⁷⁹ is highly challenging. Because of the multitude of organic building blocks and linkages, the vastness of design space for COF synthesis sets a unique opportunity to explore structure-activity relationships with the predictive potential to anticipate and tune the functional ensemble. As a matter of fact, the ideal COF-based photocatalyst, tailored for a specific reaction, might be already described in the literature, in

terms of its molecular composition and framework arrangement. In this context, the emerging power of active machine learning (AML) approaches^{80–82} will probably be of great help in assisting and accelerating the discovery of the best suitable COF-based photocatalyst, for instance by analyzing charge transport, optical absorption range, and linkage bond strength, among other specific descriptors. Indeed, fundamental photo-physical studies can provide important guidelines for photocatalytic COF design. However, COF photodynamic behavior is still underexplored and, to date, only a few seminal studies have addressed the excited-state features and decay mechanism emerging from the reticulate photoactive framework. Noteworthy, COFs can exhibit exciton transport properties that are among the highest reported for organic materials (up to 0.09 cm²/s in the case COF-5).⁸³ However, several deactivation mechanisms can occur which are derived from fast excimer formation and exciton–exciton annihilation. Therefore, a detailed analysis of the COF excited-state dynamics is instrumental to identify the type of the excited states formed and their evolution over time to charge separation, to address the nature of possible recombination events that limit efficiency.^{83,84} In this regard, controlling the excitonic effects and related properties of COF is highly desirable for application in photocatalysis, as recently shown by Jiang and co-workers, where photocatalytic terpinene oxidation has been controlled upon manipulation of the chromophore core within porphyrinic COFs.⁸⁵ Both the nature of the molecular chromophores, their integration within an extended conjugated electronic structure, or their connection via an electronically decoupled acceptor/donor heterojunction, together with the framework topology dictating distances and geometries, are expected to establish the future progress for COF application in advanced photocatalysis for the next-generation solar energy-driven organic synthesis.

AUTHOR INFORMATION

Corresponding Authors

Marcella Bonchio – Department of Chemical Sciences, University of Padova, 35131 Padova, Italy; Istituto per la Tecnologia delle Membrane, ITM-CNR, UoS di Padova, 35131 Padova, Italy; orcid.org/0000-0002-7445-0296; Email: marcella.bonchio@unipd.it

Paolo Costa – Department of Chemical Sciences, University of Padova, 35131 Padova, Italy; orcid.org/0000-0001-6324-1424; Email: paolo.costa.3@unipd.it

Authors

Alberto Vega-Peñaloza – Department of Chemical Sciences, University of Padova, 35131 Padova, Italy

Leonardo Cognigni – Department of Chemical Sciences, University of Padova, 35131 Padova, Italy

Complete contact information is available at: <https://pubs.acs.org/10.1021/acssuschemeng.1c04787>

Author Contributions

The manuscript was written through contributions of all authors.

Funding

University of Padova, Seal of Excellence @unipd QuantaCOF fellowship (P.C.) and MUR PRIN Nanoredox, Prot. 2017PBXPN4.

Notes

The authors declare no competing financial interest.

Biographies



Paolo Costa graduated with a degree in Industrial Chemistry in 2011 from the University of Padova (Italy). In 2016, he obtained his Ph.D. degree in Physical Organic Chemistry from the University of Bochum (Germany), under the supervision of Prof. Dr. Wolfram Sander. At Sander's laboratory, he focused his research on the matrix isolation studies of highly reactive intermediates and he had the opportunity to work with Dr. Gudipati at the NASA Jet Propulsion Laboratory (USA) as a visiting researcher to investigate the evolution of organic matter in amorphous water ice under radiation. After receiving the Leopoldina Fellowship award, in 2018, he joined the group of Prof. Dr. Juan C. Scaiano at the University of Ottawa (Canada) to apply single-molecule fluorescence techniques on heterogeneous catalyzed reactions. In 2020, he was awarded the MSCA-Seal of Excellence, funded by the University of Padova (Italy), to join the NanoMolCat Group led by Prof. M. Bonchio. His current research interest involves the development of bioinspired covalent organic frameworks for mimicking Photosystem II functions.



Alberto Vega-Peñaloza graduated with a degree in Pharmaceutical Chemistry at the Universidad Michoacana (Mexico). He obtained his Ph.D. at CINVESTAV-IPN, under the supervision of Prof. Eusebio Juaristi. In 2014, he joined the group of Prof. Paolo Melchiorre at ICIQ in Spain as a postdoctoral researcher. In 2018, he was awarded the MSCA-Seal of Excellence funded by the University of Padova (Italy), where he is currently appointed as a research associate. His main research interest involves the development of novel organo-catalytic and photocatalytic systems to provide sustainable synthetic methods.



Leonardo Cognigni was born in Ancona (Italy) in 1997. He obtained his M.Sc. degree in Chemistry at the University of Padova (Italy) in 2021. He is currently a Ph.D. student in Molecular Sciences under the supervision of Prof. M. Bonchio at the University of Padova. His main fields of research are the development of organic–inorganic hybrid systems, based on highly organized multichromophore arrays for artificial photosynthesis and the synthesis of new photoactive covalent organic frameworks.



Marcella Bonchio is a Full Professor of Organic Chemistry at the University of Padova, and Delegate Director and Scientific Coordinator of the National Council of Research, Institute of Membrane Technology, (ITM-CNR), section of Padova. She started her career at the University of Padova, where, in 1993, she received her Ph.D. degree in Physical Organic Chemistry. During her Ph.D. studies, she worked with Prof. J. O. Edwards at Brown University (Providence, RI, USA), followed by a postdoctoral appointment at Princeton University (Princeton, NJ, USA) with Prof. John T. Groves. Bonchio's team has established a highly interdisciplinary research program, where synthetic organic and inorganic chemistry, materials science, and physical organic methods are applied to the design of functional molecular materials. Recent achievements deal with bioinspired photosystems for water splitting and artificial photosynthesis (www.chimica.unipd.it/NanoMolCat).

ACKNOWLEDGMENTS

We acknowledge the financial support by the University of Padova (MSCA-IF Seal of Excellence @Unipd “QuantaCOF”) and Italian Ministry of University and Research (MUR PRIN “Nanoredox”, Prot. 2017PBXP4).

REFERENCES

(1) Caffarri, S.; Tibiletti, T.; Jennings, R.; Santabarbara, S. A Comparison Between Plant Photosystem I and Photosystem II

Architecture and Functioning. *Curr. Protein Pept. Sci.* **2014**, *15* (4), 296–331.

(2) Croce, R.; van Amerongen, H. Light-harvesting and structural organization of Photosystem II: From individual complexes to thylakoid membrane. *J. Photochem. Photobiol., B* **2011**, *104* (1), 142–153.

(3) Sartorel, A.; Bonchio, M.; Campagna, S.; Scandola, F. Tetrametallic molecular catalysts for photochemical water oxidation. *Chem. Soc. Rev.* **2013**, *42* (6), 2262–2280.

(4) Puntoriero, F.; Sartorel, A.; Orlandi, M.; La Ganga, G.; Serroni, S.; Bonchio, M.; Scandola, F.; Campagna, S. Photoinduced water oxidation using dendrimeric Ru(II) complexes as photosensitizers. *Coord. Chem. Rev.* **2011**, *255* (21), 2594–2601.

(5) Bonchio, M.; Syrgiannis, Z.; Burian, M.; Marino, N.; Pizzolato, E.; Dirian, K.; Rigodanza, F.; Volpato, G. A.; La Ganga, G.; Demitri, N.; Berardi, S.; Amenitsch, H.; Guldi, D. M.; Caramori, S.; Bignozzi, C. A.; Sartorel, A.; Prato, M. Hierarchical organization of perylene bisimides and polyoxometalates for photo-assisted water oxidation. *Nat. Chem.* **2019**, *11* (2), 146–153.

(6) Morris, A. J.; Meyer, G. J.; Fujita, E. Molecular Approaches to the Photocatalytic Reduction of Carbon Dioxide for Solar Fuels. *Acc. Chem. Res.* **2009**, *42* (12), 1983–1994.

(7) Romero, N. A.; Nicewicz, D. A. Organic Photoredox Catalysis. *Chem. Rev.* **2016**, *116* (17), 10075–10166.

(8) Gisbertz, S.; Pieber, B. Heterogeneous Photocatalysis in Organic Synthesis. *ChemPhotoChem.* **2020**, *4* (7), 456–475.

(9) Shaw, M. H.; Twilton, J.; MacMillan, D. W. C. Photoredox Catalysis in Organic Chemistry. *J. Org. Chem.* **2016**, *81* (16), 6898–6926.

(10) Prier, C. K.; Rankic, D. A.; MacMillan, D. W. C. Visible Light Photoredox Catalysis with Transition Metal Complexes: Applications in Organic Synthesis. *Chem. Rev.* **2013**, *113* (7), 5322–5363.

(11) Narayanam, J. M. R.; Stephenson, C. R. J. Visible light photoredox catalysis: applications in organic synthesis. *Chem. Soc. Rev.* **2011**, *40* (1), 102–113.

(12) König, B. Photocatalysis in Organic Synthesis – Past, Present, and Future. *Eur. J. Org. Chem.* **2017**, *2017* (15), 1979–1981.

(13) Vega-Peñalosa, A.; Mateos, J.; Companyó, X.; Escudero-Casao, M.; Dell'Amico, L. A Rational Approach to Organo-Photocatalysis: Novel Designs and Structure-Property Relationships. *Angew. Chem., Int. Ed.* **2021**, *60* (3), 1082–1097.

(14) Skubi, K. L.; Blum, T. R.; Yoon, T. P. Dual Catalysis Strategies in Photochemical Synthesis. *Chem. Rev.* **2016**, *116* (17), 10035–10074.

(15) Meggers, E. Exploiting Octahedral Stereocenters: From Enzyme Inhibition to Asymmetric Photoredox Catalysis. *Angew. Chem., Int. Ed.* **2017**, *56* (21), 5668–5675.

(16) Huang, X.; Lin, J.; Shen, T.; Harms, K.; Marchini, M.; Ceroni, P.; Meggers, E. Asymmetric [3 + 2] Photocycloadditions of Cyclopropanes with Alkenes or Alkynes through Visible-Light Excitation of Catalyst-Bound Substrates. *Angew. Chem., Int. Ed.* **2018**, *57* (19), 5454–5458.

(17) Shchukin, D. G.; Sviridov, D. V. Photocatalytic processes in spatially confined micro- and nanoreactors. *J. Photochem. Photobiol., C* **2006**, *7* (1), 23–39.

(18) Maiti, B.; Abramov, A.; Pérez-Ruiz, R.; Díaz Díaz, D. The Prospect of Photochemical Reactions in Confined Gel Media. *Acc. Chem. Res.* **2019**, *52* (7), 1865–1876.

(19) Hemmer, K.; Cokoja, M.; Fischer, R. A. Exploitation of Intrinsic Confinement Effects of MOFs in Catalysis. *ChemCatChem* **2021**, *13* (7), 1683–1691.

(20) Dhakshinamoorthy, A.; Asiri, A. M.; García, H. Metal–Organic Framework (MOF) Compounds: Photocatalysts for Redox Reactions and Solar Fuel Production. *Angew. Chem., Int. Ed.* **2016**, *55* (18), 5414–5445.

(21) Banerjee, T.; Gottschling, K.; Savasci, G.; Ochsenfeld, C.; Lotsch, B. V. H₂ Evolution with Covalent Organic Framework Photocatalysts. *ACS Energy Lett.* **2018**, *3* (2), 400–409.

- (22) Wang, H.; Wang, H.; Wang, Z.; Tang, L.; Zeng, G.; Xu, P.; Chen, M.; Xiong, T.; Zhou, C.; Li, X.; Huang, D.; Zhu, Y.; Wang, Z.; Tang, J. Covalent organic framework photocatalysts: structures and applications. *Chem. Soc. Rev.* **2020**, *49* (12), 4135–4165.
- (23) López-Magano, A.; Jiménez-Almarza, A.; Alemán, J.; Mas-Ballesté, R. Metal–Organic Frameworks (MOFs) and Covalent Organic Frameworks (COFs) Applied to Photocatalytic Organic Transformations. *Catalysts* **2020**, *10* (7), 720.
- (24) Vyas, V. S.; Haase, F.; Stegbauer, L.; Savasci, G.; Podjaski, F.; Ochsenfeld, C.; Lotsch, B. V. A tunable azine covalent organic framework platform for visible light-induced hydrogen generation. *Nat. Commun.* **2015**, *6* (1), 8508.
- (25) Segura, J. L.; Royuela, S.; Mar Ramos, M. Post-synthetic modification of covalent organic frameworks. *Chem. Soc. Rev.* **2019**, *48* (14), 3903–3945.
- (26) Côté, A. P.; Benin, A. I.; Ockwig, N. W.; O’Keeffe, M.; Matzger, A. J.; Yaghi, O. M. Porous, Crystalline, Covalent Organic Frameworks. *Science* **2005**, *310* (5751), 1166–1170.
- (27) Yao, C.-J.; Wu, Z.; Xie, J.; Yu, F.; Guo, W.; Xu, Z. J.; Li, D.-S.; Zhang, S.; Zhang, Q. Two-Dimensional (2D) Covalent Organic Framework as Efficient Cathode for Binder-free Lithium-Ion Battery. *ChemSusChem* **2020**, *13* (9), 2457–2463.
- (28) Guo, J.; Jiang, D. Covalent Organic Frameworks for Heterogeneous Catalysis: Principle, Current Status, and Challenges. *ACS Cent. Sci.* **2020**, *6* (6), 869–879.
- (29) Zhi, Y.; Wang, Z.; Zhang, H.-L.; Zhang, Q. Recent Progress in Metal-Free Covalent Organic Frameworks as Heterogeneous Catalysts. *Small* **2020**, *16* (24), 2001070.
- (30) Yu, F.; Liu, W.; Li, B.; Tian, D.; Zuo, J.-L.; Zhang, Q. Photostimulus-Responsive Large-Area Two-Dimensional Covalent Organic Framework Films. *Angew. Chem., Int. Ed.* **2019**, *58* (45), 16101–16104.
- (31) She, P.; Qin, Y.; Wang, X.; Zhang, Q. Recent Progress in External-Stimulus-Responsive 2D Covalent Organic Frameworks. *Adv. Mater.* **2021**, 2101175.
- (32) Bai, L.; Phua, S. Z. F.; Lim, W. Q.; Jana, A.; Luo, Z.; Tham, H. P.; Zhao, L.; Gao, Q.; Zhao, Y. Nanoscale covalent organic frameworks as smart carriers for drug delivery. *Chem. Commun.* **2016**, *52* (22), 4128–4131.
- (33) Keller, N.; Bein, T. Optoelectronic processes in covalent organic frameworks. *Chem. Soc. Rev.* **2021**, *50*, 1813–1845.
- (34) Yu, F.; Liu, W.; Ke, S.-W.; Kurmoo, M.; Zuo, J.-L.; Zhang, Q. Electrochromic two-dimensional covalent organic framework with a reversible dark-to-transparent switch. *Nat. Commun.* **2020**, *11* (1), 5534.
- (35) Lohse, M. S.; Bein, T. Covalent Organic Frameworks: Structures, Synthesis, and Applications. *Adv. Funct. Mater.* **2018**, *28* (33), 1870229.
- (36) Huang, W.; Ma, B. C.; Lu, H.; Li, R.; Wang, L.; Landfester, K.; Zhang, K. A. I. Visible-Light-Promoted Selective Oxidation of Alcohols Using a Covalent Triazine Framework. *ACS Catal.* **2017**, *7* (8), 5438–5442.
- (37) Lu, G.; Huang, X.; Li, Y.; Zhao, G.; Pang, G.; Wang, G. Covalently integrated core-shell MOF@COF hybrids as efficient visible-light-driven photocatalysts for selective oxidation of alcohols. *J. Energy Chem.* **2020**, *43*, 8–15.
- (38) Lu, G.; Huang, X.; Wu, Z.; Li, Y.; Xing, L.; Gao, H.; Dong, W.; Wang, G. Construction of covalently integrated core-shell TiO₂ nanobelts@COF hybrids for highly selective oxidation of alcohols under visible light. *Appl. Surf. Sci.* **2019**, *493*, 551–560.
- (39) Wei, P.-F.; Qi, M.-Z.; Wang, Z.-P.; Ding, S.-Y.; Yu, W.; Liu, Q.; Wang, L.-K.; Wang, H.-Z.; An, W.-K.; Wang, W. Benzoxazole-Linked Ultrastable Covalent Organic Frameworks for Photocatalysis. *J. Am. Chem. Soc.* **2018**, *140* (13), 4623–4631.
- (40) Yan, X.; Liu, H.; Li, Y.; Chen, W.; Zhang, T.; Zhao, Z.; Xing, G.; Chen, L. Ultrastable Covalent Organic Frameworks via Self-Polycondensation of an A₂B₂Monomer for Heterogeneous Photocatalysis. *Macromolecules* **2019**, *52* (21), 7977–7983.
- (41) Jiménez-Almarza, A.; López-Magano, A.; Marzo, L.; Cabrera, S.; Mas-Ballesté, R.; Alemán, J. Imine-Based Covalent Organic Frameworks as Photocatalysts for Metal Free Oxidation Processes under Visible Light Conditions. *ChemCatChem* **2019**, *11* (19), 4916–4922.
- (42) Meng, Y.; Luo, Y.; Shi, J.-L.; Ding, H.; Lang, X.; Chen, W.; Zheng, A.; Sun, J.; Wang, C. 2D and 3D Porphyrinic Covalent Organic Frameworks: The Influence of Dimensionality on Functionality. *Angew. Chem., Int. Ed.* **2020**, *59* (9), 3624–3629.
- (43) López-Magano, A.; Platero-Prats, A. E.; Cabrera, S.; Mas-Ballesté, R.; Alemán, J. Incorporation of photocatalytic Pt(II) complexes into imine-based layered covalent organic frameworks (COFs) through monomer truncation strategy. *Appl. Catal., B* **2020**, *272*, 119027.
- (44) Liu, L.; Zhang, B.; Tan, X.; Tan, D.; Cheng, X.; Han, B.; Zhang, J. Improved photocatalytic performance of covalent organic frameworks by nanostructure construction. *Chem. Commun.* **2020**, *56* (33), 4567–4570.
- (45) Sun, D.; Jang, S.; Yim, S.-J.; Ye, L.; Kim, D.-P. Metal Doped Core–Shell Metal–Organic Frameworks@Covalent Organic Frameworks (MOFs@COFs) Hybrids as a Novel Photocatalytic Platform. *Adv. Funct. Mater.* **2018**, *28* (13), 1707110.
- (46) Chen, R.; Shi, J.-L.; Ma, Y.; Lin, G.; Lang, X.; Wang, C. Designed Synthesis of a 2D Porphyrin-Based sp² Carbon-Conjugated Covalent Organic Framework for Heterogeneous Photocatalysis. *Angew. Chem., Int. Ed.* **2019**, *58* (19), 6430–6434.
- (47) Shi, J.-L.; Chen, R.; Hao, H.; Wang, C.; Lang, X. 2D sp² Carbon-Conjugated Porphyrin Covalent Organic Framework for Cooperative Photocatalysis with TEMPO. *Angew. Chem., Int. Ed.* **2020**, *59* (23), 9088–9093.
- (48) Liu, Z.; Su, Q.; Ju, P.; Li, X.; Li, G.; Wu, Q.; Yang, B. A hydrophilic covalent organic framework for photocatalytic oxidation of benzylamine in water. *Chem. Commun.* **2020**, *56* (5), 766–769.
- (49) Wang, Y.; Liu, H.; Pan, Q.; Wu, C.; Hao, W.; Xu, J.; Chen, R.; Liu, J.; Li, Z.; Zhao, Y. Construction of Fully Conjugated Covalent Organic Frameworks via Facile Linkage Conversion for Efficient Photoenzymatic Catalysis. *J. Am. Chem. Soc.* **2020**, *142* (13), 5958–5963.
- (50) Liu, W.; Su, Q.; Ju, P.; Guo, B.; Zhou, H.; Li, G.; Wu, Q. A Hydrazone-Based Covalent Organic Framework as an Efficient and Reusable Photocatalyst for the Cross-Dehydrogenative Coupling Reaction of N-Aryltetrahydroisoquinolines. *ChemSusChem* **2017**, *10* (4), 664–669.
- (51) Tian, M.; Liu, S.; Bu, X.; Yu, J.; Yang, X. Covalent Organic Frameworks: A Sustainable Photocatalyst toward Visible-Light-Accelerated C3 Arylation and Alkylation of Quinoxalin-2(1H)-Ones. *Chem. - Eur. J.* **2020**, *26* (2), 348–348.
- (52) Liu, S.; Pan, W.; Wu, S.; Bu, X.; Xin, S.; Yu, J.; Xu, H.; Yang, X. Visible-light-induced tandem radical addition–cyclization of 2-aryl phenyl isocyanides catalysed by recyclable covalent organic frameworks. *Green Chem.* **2019**, *21* (11), 2905–2910.
- (53) Yuan, J.; Xia, Q.; Zhu, W.; Wu, C.; Wang, B.; Liu, B.; Yang, X.; Xu, Y.; Xu, H. Sunlight-Driven Synthesis of 1,2,4-Thiadiazoles via Oxidative Construction of a Nitrogen-Sulfur Bond Catalyzed by a Reusable Covalent Organic Framework. *ChemPhotoChem.* **2020**, *4* (6), 445–450.
- (54) Zhi, Y.; Li, Z.; Feng, X.; Xia, H.; Zhang, Y.; Shi, Z.; Mu, Y.; Liu, X. Covalent organic frameworks as metal-free heterogeneous photocatalysts for organic transformations. *J. Mater. Chem. A* **2017**, *5* (44), 22933–22938.
- (55) Liu, H.; Li, C.; Li, H.; Ren, Y.; Chen, J.; Tang, J.; Yang, Q. Structural Engineering of Two-Dimensional Covalent Organic Frameworks for Visible-Light-Driven Organic Transformations. *ACS Appl. Mater. Interfaces* **2020**, *12* (18), 20354–20365.
- (56) Kang, X.; Wu, X.; Han, X.; Yuan, C.; Liu, Y.; Cui, Y. Rational synthesis of interpenetrated 3D covalent organic frameworks for asymmetric photocatalysis. *Chem. Sci.* **2020**, *11* (6), 1494–1502.
- (57) Li, Z.; Zhi, Y.; Shao, P.; Xia, H.; Li, G.; Feng, X.; Chen, X.; Shi, Z.; Liu, X. Covalent organic framework as an efficient, metal-free,

heterogeneous photocatalyst for organic transformations under visible light. *Appl. Catal., B* **2019**, *245*, 334–342.

(58) Tian, M.; Wang, Y.; Bu, X.; Wang, Y.; Yang, X. An ultrastable olefin-linked covalent organic framework for photocatalytic decarboxylative alkylations under highly acidic conditions. *Catal. Sci. Technol.* **2021**, *11*, 4272–4279.

(59) Chen, H.; Liu, W.; Laemont, A.; Krishnaraj, C.; Feng, X.; Rohman, F.; Meledina, M.; Zhang, Q.; Van Deun, R.; Leus, K.; Van Der Voort, P. A Visible-Light-Harvesting Covalent Organic Framework Bearing Single Nickel Sites as a Highly Efficient Sulfur–Carbon Cross-Coupling Dual Catalyst. *Angew. Chem., Int. Ed.* **2021**, *60* (19), 10820–10827.

(60) Ohara, K.; Inokuma, Y.; Fujita, M. The Catalytic Z to E Isomerization of Stilbenes in a Photosensitizing Porous Coordination Network. *Angew. Chem., Int. Ed.* **2010**, *49* (32), 5507–5509.

(61) Haug, W. K.; Moscarello, E. M.; Wolfson, E. R.; McGrier, P. L. The luminescent and photophysical properties of covalent organic frameworks. *Chem. Soc. Rev.* **2020**, *49* (3), 839–864.

(62) Steckhan, E.; Herrmann, S.; Ruppert, R.; Dietz, E.; Frede, M.; Spika, E. Analytical study of a series of substituted (2,2'-bipyridyl)-(pentamethylcyclopentadienyl)rhodium and -iridium complexes with regard to their effectiveness as redox catalysts for the indirect electrochemical and chemical reduction of NAD(P)⁺. *Organometallics* **1991**, *10* (5), 1568–1577.

(63) Sheldon, R. A.; Arends, I.; Hanefeld, U. *Green Chemistry and Catalysis*; Wiley–VCH Verlag GmbH & Co. KGaA: Weinheim, Germany, 2007.

(64) Margrey, K. A.; Czaplyski, W. L.; Nicewicz, D. A.; Alexanian, E. J. A General Strategy for Aliphatic C–H Functionalization Enabled by Organic Photoredox Catalysis. *J. Am. Chem. Soc.* **2018**, *140* (12), 4213–4217.

(65) Uygur, M.; García Mancheño, O. Visible light-mediated organophotocatalyzed C–H bond functionalization reactions. *Org. Biomol. Chem.* **2019**, *17* (22), 5475–5489.

(66) Nicewicz, D. A.; MacMillan, D. W. C. Merging Photoredox Catalysis with Organocatalysis: The Direct Asymmetric Alkylation of Aldehydes. *Science* **2008**, *322* (5898), 77–80.

(67) Silvi, M.; Melchiorre, P. Enhancing the potential of enantioselective organocatalysis with light. *Nature* **2018**, *554* (7690), 41–49.

(68) Gualandi, A.; Marchini, M.; Mengozzi, L.; Natali, M.; Lucarini, M.; Ceroni, P.; Cozzi, P. G. Organocatalytic Enantioselective Alkylation of Aldehydes with [Fe(bpy)₃]Br₂ Catalyst and Visible Light. *ACS Catal.* **2015**, *5* (10), 5927–5931.

(69) Riente, P.; Matas Adams, A.; Albero, J.; Palomares, E.; Pericàs, M. A. Light-Driven Organocatalysis Using Inexpensive, Nontoxic Bi₂O₃ as the Photocatalyst. *Angew. Chem., Int. Ed.* **2014**, *53* (36), 9613–9616.

(70) Neumann, M.; Földner, S.; König, B.; Zeitler, K. Metal-Free, Cooperative Asymmetric Organophotoredox Catalysis with Visible Light. *Angew. Chem., Int. Ed.* **2011**, *50* (4), 951–954.

(71) Bhadra, M.; Kandambeth, S.; Sahoo, M. K.; Addicoat, M.; Balaraman, E.; Banerjee, R. Triazine Functionalized Porous Covalent Organic Framework for Photo-organocatalytic E–Z Isomerization of Olefins. *J. Am. Chem. Soc.* **2019**, *141* (15), 6152–6156.

(72) Almquist, C. B.; Biswas, P. Role of Synthesis Method and Particle Size of Nanostructured TiO₂ on Its Photoactivity. *J. Catal.* **2002**, *212* (2), 145–156.

(73) Colson, J. W.; Woll, A. R.; Mukherjee, A.; Levendorf, M. P.; Spittler, E. L.; Shields, V. B.; Spencer, M. G.; Park, J.; Dichtel, W. R. Oriented 2D Covalent Organic Framework Thin Films on Single-Layer Graphene. *Science* **2011**, *332* (6026), 228–231.

(74) Sun, B.; Liu, J.; Cao, A.; Song, W.; Wang, D. Interfacial synthesis of ordered and stable covalent organic frameworks on amino-functionalized carbon nanotubes with enhanced electrochemical performance. *Chem. Commun.* **2017**, *53* (47), 6303–6306.

(75) Moya, A.; Hernando-Pérez, M.; Pérez-Illana, M.; San Martín, C.; Gómez-Herrero, J.; Alemán, J.; Mas-Ballesté, R.; de Pablo, P. J. Multifunctional carbon nanotubes covalently coated with imine-based

covalent organic frameworks: exploring structure–property relationships through nanomechanics. *Nanoscale* **2020**, *12* (2), 1128–1137.

(76) Gomes, R.; Bhattacharyya, A. J. Carbon Nanotube-Templated Covalent Organic Framework Nanosheets as an Efficient Sulfur Host for Room-Temperature Metal–Sulfur Batteries. *ACS Sustainable Chem. Eng.* **2020**, *8* (15), 5946–5953.

(77) DeSantis, D.; Mason, J. A.; James, B. D.; Houchins, C.; Long, J. R.; Veenstra, M. Techno-economic Analysis of Metal–Organic Frameworks for Hydrogen and Natural Gas Storage. *Energy Fuels* **2017**, *31* (2), 2024–2032.

(78) Peng, Y.; Wong, W. K.; Hu, Z.; Cheng, Y.; Yuan, D.; Khan, S. A.; Zhao, D. Room Temperature Batch and Continuous Flow Synthesis of Water-Stable Covalent Organic Frameworks (COFs). *Chem. Mater.* **2016**, *28* (14), 5095–5101.

(79) Haase, F.; Lotsch, B. V. Solving the COF trilemma: towards crystalline, stable and functional covalent organic frameworks. *Chem. Soc. Rev.* **2020**, *49* (23), 8469–8500.

(80) Coley, C. W.; Green, W. H.; Jensen, K. F. Machine Learning in Computer-Aided Synthesis Planning. *Acc. Chem. Res.* **2018**, *51* (5), 1281–1289.

(81) Kunkel, C.; Margraf, J. T.; Chen, K.; Oberhofer, H.; Reuter, K. Active discovery of organic semiconductors. *Nat. Commun.* **2021**, *12* (1), 2422.

(82) Yang, P.; Zhang, H.; Lai, X.; Wang, K.; Yang, Q.; Yu, D. Accelerating the Selection of Covalent Organic Frameworks with Automated Machine Learning. *ACS Omega* **2021**, *6* (27), 17149–17161.

(83) Flanders, N. C.; Kirschner, M. S.; Kim, P.; Fauvell, T. J.; Evans, A. M.; Helweh, W.; Spencer, A. P.; Schaller, R. D.; Dichtel, W. R.; Chen, L. X. Large Exciton Diffusion Coefficients in Two-Dimensional Covalent Organic Frameworks with Different Domain Sizes Revealed by Ultrafast Exciton Dynamics. *J. Am. Chem. Soc.* **2020**, *142* (35), 14957–14965.

(84) Jakowetz, A. C.; Hinrichsen, T. F.; Ascherl, L.; Sick, T.; Calik, M.; Auras, F.; Medina, D. D.; Friend, R. H.; Rao, A.; Bein, T. Excited-State Dynamics in Fully Conjugated 2D Covalent Organic Frameworks. *J. Am. Chem. Soc.* **2019**, *141* (29), 11565–11571.

(85) Qian, Y.; Li, D.; Han, Y.; Jiang, H.-L. Photocatalytic Molecular Oxygen Activation by Regulating Excitonic Effects in Covalent Organic Frameworks. *J. Am. Chem. Soc.* **2020**, *142* (49), 20763–20771.